Supplementary Information

Modulating Electric Field Distribution by Alkali Cations for CO_2 Electroreduction in Strongly Acidic Medium

Jun Gu [1,2], Shuo Liu [3], Weiyan Ni [1], Wenhao Ren [1], Sophia Haussener, [3] and Xile Hu [1]*

Affiliation:

1. Laboratory of Inorganic Synthesis and Catalysis, Institute of Chemical Sciences and Engineering, Ecole Polytechnique Fédérale de Lausanne (EPFL), EPFL-ISIC-LSCI, BCH 3305, Lausanne, CH 1015 Switzerland.
2. Department of Chemistry, Southern University of Science and Technology, Shenzhen, Guangdong, 518055, China.
3. Laboratory of Renewable Energy Science and Engineering, Institute of Mechanical Engineering, École Polytechnique Fédérale de Lausanne, 1015 Lausanne, Switzerland.

* Corresponding author. E-mail: xile.hu@epfl.ch

Contents	Page
Supplementary Methods	2-6
Supplementary Note 1. Carbon Efficiency and Energy Consumption Estimation	7-14
Supplementary Note 2. Simulation procedure	15-20
Supplementary Figures 1-26	21-46
Supplementary Tables 1-4	47-50
Supplementary References	51-52

Supplementary Methods

Electrochemical Measurements:

Electrolyte solutions: Deionized water was used for the preparation of electrolyte solutions. Sulfuric acid (H_2SO_4, 95%, Merck), lithium sulfate (Li_2SO_4, 99%, Roth), sodium sulfate decahydrate ($Na_2SO_4 \cdot 10H_2O$, 99%, Sigma-Aldrich) and potassium sulfate (K_2SO_4, 99%, ABCR) were used to prepare solutions of 0.1 M H_2SO_4 and 0.1 M H_2SO_4 + 0.4 M M_2SO_4 (M = Li, Na and K). Sulfuric acid and cesium hydroxide monohydrate ($CsOH \cdot H_2O$, 99%, Sigma-Aldrich) were used to prepare solution of 0.1 M H_2SO_4 + 0.4 M Cs_2SO_4. Trifluoromethanesulfonic acid (HOTf, 99%, Fluorochem), lithium trifluoromethanesulfonate (LiOTf, 98%, Acros), sodium trifluoromethanesulfonate (NaOTf, 98%, Acros) and potassium trifluoromethanesulfonate (KOTf, 99%, Fluorochem) were used to prepare solutions of 0.1 M HOTf and 0.1 M HOTf + 0.4 M MOTf (M = Li, Na and K). HOTf and cesium hydroxide monohydrate were used to prepare solution of 0.1 M HOTf + 0.4 M CsOTf. Potassium bicarbonate ($KHCO_3$, 99.7%, Sigma-Aldrich) was used to prepare 0.8 M $KHCO_3$. Potassium hydroxide (KOH, 1 $mol \cdot L^{-1}$ solution, Merck) was used to prepare 0.8 M KOH.

Detection of products: Gas phase products were detected online by gas chromatography (GC). H_2 and CO were detected by a homemade GC equipped with a Carboxen®-1010 PLOT capillary column and a thermal conductivity detector (TCD, VICI). Helium was used as the carrier gas for the analysis of CO and argon was used for the analysis of H_2. The temperature program was: keeping at 35 °C for 3 minutes; heating to 80 °C with a ramping rate of 20 $°C \cdot min^{-1}$; keeping at 80 °C for 5 minutes.

Methane, ethylene and propene were detected by a Claurus 400 GC (Perkin Elmer) equipped with a Porapak Q column (Agilent) and a flame ionization detector (FID). H_2 was used as the carrier gas. The temperature program was: keeping at 50 °C for 5 minutes; heating to 150 °C with a ramping rate of 20 $°C \cdot min^{-1}$; keeping at 150 °C for

10 minutes.

^{1}H-nuclear magnetic resonance (^{1}H-NMR, 400 MHz, Bruker) was used to detect the solution phase products after chronoamperometry tests. Dimethyl sulfoxide (DMSO) was used as an inner standard to quantify the products. 30.7 μL of DMSO dissolved in 70 mL of deionized water was used as the standard solution (6.17 mmol·L^{-1}). For each test, 400 μL of the electrolyte for working electrode, 40 μL of DMSO standard solution and 50 μL of deuterium oxide (D_2O) were mixed.

Supplementary Fig. 5b-e show the GC-TCD curves with He and Ar as the carrier gas, the GC-FID curve, and the ^{1}H-NMR spectrum of catholyte for Cu/C, respectively. The electrolyte was 0.1 M H_2SO_4 + 0.4 M K_2SO_4. The chronoamperometry test was conducted at -1.41 V vs RHE for 30 minutes.

Calculation of Faradaic efficiency and partial current density: The Faradaic efficiency of a gas product *g* was calculated according to the equation:

$$\mathrm{FE}_g = \frac{N_g \cdot r_g \cdot F}{I} = \frac{N_g p f x_g F/RT}{I} \quad (1)$$

In this equation, N_g is the number of electrons transferred to produce one molecule of *g*. For H_2, CO, methane, ethylene and propene, N_g equals 2, 2, 8, 12 and 18, respectively. r_g is the formation rate of *g* (unit: mol·s^{-1}). *F* is the Faraday constant (9.65 × 10^4 C·mol^{-1}). *I* is current. x_g is the fraction of gas *g* detected by GC. *f* is the mass flow rate of gas flow (unit: sccm). *p* is 101 kPa and *T* is 273 K. *R* is the gas constant (8.314 J·mol^{-1}·K^{-1}).

The Faradaic efficiency of a solution-phase product *s* was calculated according to the equation:

$$\mathrm{FE}_s = \frac{N_s \cdot n_s \cdot F}{Q} = N_s \cdot \frac{6 \cdot c_{\mathrm{DMSO}} \cdot V_{\mathrm{DMSO}} \cdot A_{s,H}}{N_{s,H}} \cdot \frac{V_{\mathrm{ele}}}{V_{\mathrm{NMR}}} \cdot F/Q \quad (2)$$

In this equation, N_s is the number of electrons transferred to produce one molecule of *s*. For formic acid, acetic acid, ethanol and 1-propanol, N_s equals 2, 8, 12 and 18,

respectively. n_s is the total amount of *s* generated in one chronoamperometry test (unit: mol). Q is the integrated charge of one test (unit: C). c_{DMSO} is the concentration of DMSO in standard solution (6.17 mmol·L^{-1}) and V_{DMSO} is the volume of standard solution (40 μL). $A_{s,H}$ is the relative area of the peak in ^{1}H-NMR spectrum used for quantification of *s* with respect to the peak of 6 H atoms of DMSO. For ethanol and 1-propanol, the peaks of methyl groups were used for quantification. $N_{s,H}$ is the number of H atoms in one *s* molecule used for quantification. For formic acid, acetic acid, ethanol and 1-propanol, $N_{s,H}$ equals 1, 3, 3 and 3, respectively. V_{ele} is the volume of electrolyte for working electrode and V_{NMR} is the volume of electrolyte used for NMR test.

The partial current density of product *p* was calculated according to the equation:

$$j_p = j \cdot FE_p \quad (3)$$

In this equation, *j* is the current density normalized to the area of working electrode.

Production of aqueous solution of pure formic acid: SnO_2/C was used as the catalyst in the three-electrode cell. Nafion® 211 and Fumasep® FAA-3-50 membranes were used for 0.1 M H_2SO_4 + 0.4 M K_2SO_4 and 0.8 M $KHCO_3$, respectively. The volumes of both catholyte and anolyte solutions were 10 mL, and both of them were circulated with a flow rate of 5 mL·min^{-1}. Chronoamperometry tests at -1.5 V vs SHE for 15000 seconds were conducted, as shown in Supplementary Fig. 4. After the electrolysis, the volume of the electrolyte for working electrode was adjusted to 10 mL by adding deionized water. 40 μL of this electrolyte, 40 μL of DMSO standard solution, 50 μL of D_2O and 360 μL of deionized water were mixed for ^{1}H-NMR test. The electrolyte solution was then loaded in a 25-mL flask and heated by an oil bath at 150 °C. The distillate was collected until all the water in the flask was evaporated. The volume of the distillate was adjusted to 10 mL by adding deionized water and the sample for ^{1}H-NMR test was prepared with the same method.

Two-electrode flow cell: Supplementary Fig. 6a shows the scheme of the two-

electrode flow cell. CeTech W1S1009 carbon cloths were used as both cathode and anode. Au/C and IrO_2 were used as catalysts for cathode and anode, respectively. A titanium plate was used as current collector for both electrodes. An EPDM plate with the thickness of 1.5 mm was used as the chamber of electrolyte solution. The effective window for electrolysis was a circle with the diameter of 1.13 cm (area = 1 cm^2). Kapton tapes with circular windows with the same size was pasted on both electrodes to control the effective area exposed to the electrolyte. No membrane was used between cathode and anode and two electrodes shared the same electrolyte. CO_2 and He streams were supplied behind cathode and anode, respectively. The volume of electrolyte solution was 10 mL, which was circulated with the flow rate of 1 $mL \cdot min^{-1}$. For each kind of electrolyte, chronopotentiometry test at 200 $mA \cdot cm^{-2}$ was conducted for 15000 seconds. No *iR* compensation was used when recording the cell voltage. The flow rates of CO_2 and He were 100 sccm and 6 sccm, respectively. CO was detected by online GC analysis. The electrochemical impedance spectroscopy tests were conducted at open circuit potential with an amplitude of 10 mV from 300 kHz to 0.1 Hz.

Tests of dissolution of Sn and Cu: The weight ratios of Sn and Cu in SnO_2/C and Cu/C were probed by thermogravimetric analysis in air. SnO_2/C and Cu/C loaded on GDE were used for the stability test. The loading of catalysts was measured by the mass change of GDE before and after spraying the catalysts. The tests were done in a three-electrode flow cell shown in Supplementary Fig. 2. 0.1 M H_2SO_4 + 0.4 M K_2SO_4, 0.8 M $KHCO_3$, and 0.8 M KOH were used as acidic, near neutral, and alkaline electrolyte solutions, respectively. Chronopotentiometry test at -200 $mA \cdot cm^{-2}$ was conducted for 15000 seconds for each medium. After electrolysis, the near neutral and alkaline catholyte was acidified by ultrapure nitric acid. The volume of catholyte was then adjusted to 25.0 mL for the ICP-MS test. Supplementary Table 1 shows the concentration of Sn and Cu dissolved into electrolyte solution during electrolysis. Catalysts after electrolysis were dispersed in ethanol and dropped on Cu grid for TEM characterization (Supplementary Fig. 7).

Rotating disk electrode experiments: The limiting diffusion current density of the reduction of hydronium ions was calculated according to Levich equation[1] (dashed horizontal lines in Fig. 4a and Supplementary Fig. 14):

$$j_{d,H^+} = 0.62FD_{H^+}^{2/3}\nu^{-1/6}c_{0,H^+}\omega^{1/2} \quad (4)$$

In this equation, F is the Faraday constant (9.65×10^4 C·mol^{-1}), D_{H+} is the diffusion coefficient of hydronium ions (9.3×10^{-5} cm^2·s^{-1})[2], ν is the kinematic viscosity of electrolyte (0.01 cm^2·s^{-1})[3], $c_{0,H+}$ is the bulk concentration of hydronium ions (0.1 M), and ω is the rotating speed of the RDE (unit: rad·s^{-1}).

Supplementary Note 1 | Carbon Efficiency and Energy Consumption Estimation

Supplementary Fig. 8a-d shows the schemes and electrode reactions of sustainable electrolyzer systems for CO_2 reduction to produce CO or ethylene based on flow cells with 0.1 M H_2SO_4 + 0.4 M K_2SO_4, 0.5 M $KHCO_3$, and 1 M KOH solutions as media as well as an MEA with an anion exchange membrane, respectively. We assume HER as the only side reaction. Theoretical carbon efficiency is estimated by assuming the Faradaic efficiency for the aiming product is 100% and all CO_2 is consumed.

Acidic medium: In acidic medium, CO_3^{2-} ions are formed due to the local pH increase near the cathode. However, the as-formed CO_3^{2-} ions are protonated by hydronium ions diffusing from the bulk solution so CO_2 molecules are released and can be reduced by the cathode again.[4] A pressure swing adsorption (PSA) separation unit[5,6] is added at the outlet of cathode to separate the aiming product (CO or ethylene), side product (H_2) and unreacted CO_2. CO_2 is recycled to the inlet of the cathode (Supplementary Fig. 8a). Since CO_3^{2-} ions don't not penetrate the acidic medium, the theoretical carbon efficiency is 100%.

Near neutral medium: In near neutral medium, OH^- ions are formed during cathodic reactions including CO_2 reduction and HER. OH^- ions reacted with CO_2 to form CO_3^{2-} ions. The net reactions for CO and ethylene formation at the cathode are shown in Supplementary Fig. 8b. CO_3^{2-} ions penetrate the electrolyte and are finally protonated at the anode to release a mixture of O_2 and CO_2. For CO formation, 1 out of 2 CO_2 molecules forms CO_3^{2-} ions, and for ethylene formation, 6 out of 8 CO_2 molecules form CO_3^{2-} ions. Therefore, the theoretical carbon efficiencies for CO and ethylene formation in near neutral medium are 50% and 25%, respectively. When taking HER side reaction into consideration (since HER also generates OH^- ions at the cathode which react with CO_2) the carbon efficiency further decreases as the Faradaic efficiency of CO_2 reduction decreases. PSA separation units are added at the cathode outlet and anode outlet and CO_2 separated from the gas mixture from both electrodes is recycled to the inlet of cathode.

Alkaline medium: In alkaline medium, CO_2 molecules react with OH^- ions in the electrolyte ($CO_2 + OH^- \rightarrow HCO_3^-$). Since the electrolyte solution is refreshed constantly, we assume the reaction between CO_2 and OH^- ions reaches a steady state and the consumption rate of CO_2 is constant over time. At a certain position near the cathode, the consumption rate of CO_2 equales the CO_2 accumulation rate due to diffusion:

$$D_{CO2}\frac{d^2c}{dx^2} = kc[OH^-] \quad (5)$$

where x is the distance from the gas-solution interface, c is the concentration of CO_2 at the point, D_{CO2} is the diffusion coefficient of CO_2 in water (1.91×10^{-9} $m^2\cdot s^{-1}$),[7] k is the rate constant of the reaction between CO_2 and OH^- ion (2.23 $mol^{-1}\cdot m^3\cdot s^{-1}$).[8] We assume the concentration of OH^- consumed by the reaction can be neglected compared to the initial concentration of OH^- (1 M) as long as the refreshing of the electrolyte solution is fast enough. Thus, we take $[OH^-]$ = 1 M as a constant. Then, we have:

$$c = c_0 \cdot \exp(-\sqrt{\frac{k[OH^-]}{D_{CO2}}} \cdot x) \quad (6)$$

where c_0 is the concentration of CO_2 at the gas-solution interface, which we assume as the solubility of CO_2 in water (0.038 M).[9] The consumption rate of CO_2 by this neutralization reaction in a unit area is:

$$J_n = -D_{CO2} \cdot \frac{dc}{dx} = c_0 \cdot \sqrt{kD_{CO2}[OH^-]} = 7.84 \times 10^{-6} mol \cdot s^{-1} \cdot cm^{-2} \quad (7)$$

The consumption rate of CO_2 by the CO_2 reduction reaction in a unit area is:

$$J_r = \frac{n \cdot j_{CO2}}{z \cdot F} \quad (8)$$

where j_{CO2} is the partial current density of CO_2 reduction, n is the number of CO_2 molecules involved in the reaction (n = 1 for CO formation and n = 2 for ethylene formation), z is the number of electrons involved in the reaction (z =2 for CO formation and z = 12 for ethylene formation), and F is the Faradaic constant (96485 $C\cdot mol^{-1}$). The carbon efficiency is calculated according to:

$$\text{Carbon efficiency} = J_r / (J_r + J_n) \times 100\% \quad (9)$$

We assume the partial current density of CO_2 reduction is 200 $mA \cdot cm^{-2}$, which represents a state-of-the-art partial current density. Thus, the carbon efficiency in 1 M KOH is 11.7% for CO formation and 4.2% for ethylene formation. As the partial current density of CO_2 reduction decreases, the carbon efficiency decreases. For a sustainable system in Supplementary Fig. 8c, a unit to regenerate KOH and CO_2 from K_2CO_3[10] is needed at the outlet of solution flow and a PSA separation unit is needed at the outlet of cathode. CO_2 from these two units is recycled to the inlet of cathode.

Membrane electrode assembly based on anion exchange membrane: The MEA setup of Berlinguette and co-workers[11] is used as the electrolyzer in Supplementary Fig. 8d, where a Sustainion membrane is used as the anion exchange membrane and 1 M KOH is used as the anolyte. The reactions at the cathode in the MEA setup are similar to those in the flow cell with near neutral medium. The charge carrier in the anion exchange membrane is CO_3^{2-} ions instead of OH^- ions due to the CO_2 atmosphere in the cathode chamber. The theoretical carbon efficiencies for CO and ethylene formation are 50% and 25%, respectively. The outlet flow of the anode chamber contains O_2 gas and the electrolyte solution containing K_2CO_3 and KOH. A unit to regenerate KOH and CO_2 is added at the outlet of the anode chamber and a PSA separation unit is added at the outlet of the cathode chamber. CO_2 from these two units is recycled to the inlet of cathode.

Energy estimation: As shown in Fig. 3, the energy consumption to produce 1 mole of CO or ethylene is divided into 7 parts: equilibrium, cathode energy loss, anode energy loss, Ohmic loss, side reaction, gas separation and electrolyte regeneration. The energy consumption is calculated by assuming the partial current density of CO_2 reduction is 200 $mA \cdot cm^{-2}$. 0.1 M H_2SO_4 + 0.4 M K_2SO_4 (pH = 1.5), 0.5 M $KHCO_3$ (pH = 7.2) and 1 M KOH (pH = 13.6) are selected as acidic, near neutral and alkaline electrolytes, respectively.

Equilibrium corresponds to the change of Gibbs free energy of the overall reaction. It was calculated according to:

$$\Delta G_m = zF(\varphi_{\mathrm{O2/H2O}} - \varphi_{\mathrm{CO/product}}) \quad (10)$$

where z is the number of electrons involved in the production of one product molecule, $\varphi_{\mathrm{O2/H2O}}$ is the equilibrium electrode potential for OER (1.23 V vs RHE) and $\varphi_{\mathrm{CO/product}}$ is the equilibrium electrode potential for CO_2 reduction (-0.11 V vs RHE for CO formation and 0.07 V vs RHE for ethylene formation) at standard conditions.[12] Therefore, the 'equilibrium' term is 260 kJ·mol^{-1} for CO formation and 1338 kJ·mol^{-1} for ethylene formation.

Cathode energy loss is due to the overpotential of CO_2 reduction. As indicated by Supplementary Fig. 11, the potentials for CO_2 reduction with a certain partial current density in different media are approximately identical in SHE scale. We assume the potential for CO formation with a partial current density of 200 mA·cm^{-2} is -1.20 V vs SHE. The equilibrium potential of CO_2/CO is -0.11 V vs RHE. Thus, the overpotential of CO formation is:

$$\eta_{\mathrm{CO,@200mA\cdot cm^{-2}}} = -0.11\mathrm{V} - 0.0592\mathrm{V/pH} \cdot \mathrm{pH} - (-1.20\mathrm{V})$$

$$= 1.09\mathrm{V} - 0.0592\mathrm{V/pH} \cdot \mathrm{pH} \quad (11)$$

Then, the cathodic energy loss was calculated according to:

$$\Delta E_{\mathrm{cathode}} = 2F\eta_{\mathrm{CO@200mA\cdot cm^{-2}}} \quad (12)$$

Similarly, we assume the potential for ethylene formation with a partial current density of 200 mA·cm^{-2} is -1.26 V vs SHE, according to the performance of the state-of-the-art Cu-based catalyst.[13] The equilibrium potential of CO_2/ethylene is 0.07 V vs RHE. Thus, the overpotential of CO formation is:

$$\eta_{\mathrm{C2H4@200mA\cdot cm^{-2}}} = 0.07\mathrm{V} - 0.0592\mathrm{V/pH} \cdot \mathrm{pH} - (-1.26\mathrm{V})$$

$$= 1.33\mathrm{V} - 0.0592\mathrm{V/pH} \cdot \mathrm{pH} \quad (13)$$

The cathode energy loss is calculated according to:

$$\Delta E_{\mathrm{cathode}} = 12F\eta_{\mathrm{C2H4@200mA\cdot cm^{-2}}} \quad (14)$$

For an MEA setup, as we discussed in previous section, the anions in AEM are in CO_3^{2-} form and the cathode is in CO_2 atmosphere. Therefore, the cathodic overpotential was estimated in a near neutral condition (pH = 7.2).

Anode energy loss is due to the overpotential of OER. Ru-N-C single atom catalyst,[14] $RuIrCaO_x$ catalyst[15] and Ni-Fe-based nanowire arrays[16] were chosen as the state-of-the-art OER catalysts work in acidic, near neutral, and alkaline media, respectively. The potentials for a current density of 200 $mA \cdot cm^{-2}$ on these three catalysts were 1.58 V vs RHE, 1.92 V vs RHE and 1.47 V vs RHE, respectively. Hence, the overpotentials of OER in acidic, near neutral and alkaline media were 0.35 V, 0.69 V and 0.24 V, respectively. The anode energy loss is calculated according to:

$$\Delta E_{\text{anode}} = zF\eta_{\text{OER}} \tag{15}$$

Ohmic loss is caused by the resistance of the electrolyte solution or anion exchange membrane between cathode and anode. The potential drop due to the resistance is calculated according to:

$$IR = jA \cdot \frac{L}{A\sigma} = \frac{jL}{\sigma} \tag{16}$$

where j is the current density (200 $mA \cdot cm^{-2}$), A is the effective area of the electrode, L is the distance between two electrodes, σ is the specific conductivity of the electrolyte solution or membrane. We use L = 1 mm for the thickness of the electrolyte solution in flow cell and L = 60 μm for the thickness of the membrane in MEA. The specific conductivity of 0.1 M H_2SO_4 + 0.4 M K_2SO_4 solution is 0.15 $S \cdot cm^{-1}$ according to Supplementary Fig. 12a, and those of 0.5 M $KHCO_3$ solution, 1 M KOH solution and AEM (Sustainion) are 0.05 $S \cdot cm^{-1}$,[17] 0.21 $S \cdot cm^{-1}$ [18] and 0.024 $S \cdot cm^{-1}$,[19] respectively. Note that the specific conductivity value of AEM with CO_3^{2-} ions as charge carrier is used. The energy loss due to resistance is then calculated according to:

$$\Delta E_{\text{Ohmic}} = zF\frac{jL}{\sigma} \tag{17}$$

Side reaction term corresponds to the energy consumption used for the production of side product as 1 mole of aiming product forms, and is calculated according to:

$$\Delta E_{\text{side}} = (\Delta G_m + \Delta E_{\text{cathode}} + \Delta E_{\text{anode}} + \Delta E_{\text{Ohmic}}) \cdot \frac{100\%-\text{FE}\%}{\text{FE}\%} \quad (18)$$

where FE% is the Faradaic efficiency of the aiming product. For CO and ethylene production, we set FE% equaled 90% and 70%, respectively, according to the performance of the state-of-the-art catalysts.[13,20]

Gas separation term corresponds to the energy consumption needed to separate the gas mixture from the cathode in every system and from the anode in a flow cell with near neutral medium, as shown in Supplementary Fig. 8. PSA unit is used for the separation and the energy consumption is 0.25 kWh·m^{-3}.[5,6] It is reported that the recovery rate for a PSA unit is 90%.[21] This would lead to a decrease of carbon efficiency of the whole system. We assumed HER is the only side reaction on cathode, then, to produce 1 mole of aiming product, the mole of H_2 is:

$$n_{\text{H2}} = 1\text{mol} \cdot \frac{z\cdot(100\%-\text{FE}\%)}{2\cdot\text{FE}\%} \quad (19)$$

We assume the molar ratio of unreacted CO_2 in the outlet gas from cathode is 20%. Then, to produce 1 mole of aiming product, the mole of outlet gas from cathode was:

$$n_{\text{cathode}} = (1\text{mol} + n_{\text{H2}}) \cdot \frac{100\%}{100\%-20\%} \quad (20)$$

For a flow cell in near neutral medium, as shown in Supplementary Fig. 8b, to produce 1 mole of aiming product, the mole of outlet gas from anode is:

$$n_{\text{anode}} = 1\text{mol} \cdot z \cdot \frac{100\%}{\text{FE}\%} \cdot \frac{3}{4} \quad (21)$$

For the other setups, a PSA unit is not used for the outlet of anode. So, we set n_{anode} = 0. Thus, to produce 1 mole of aiming product, the energy consumption for gas separation is:

$$\Delta E_{\text{separation}} = (n_{\text{cathode}} + n_{\text{anode}}) \cdot 22.4\text{L} \cdot \text{mol}^{-1} \cdot 0.25\text{kWh} \cdot \text{m}^{-3} \quad (22)$$

Electrolyte regeneration term is the energy consumption to convert K_2CO_3 into CO_2 and KOH, which is necessary for flow cell in alkaline medium (Supplementary Fig. 8c) or with an MEA (Supplementary Fig. 8d). A calcium caustic loop[10] is used for this purpose and the energy consumption for this step is 194.7 $kJ \cdot mol_{CO2}^{-1}$. For a flow cell in alkaline medium, the carbon efficiency is calculated according to Supplementary Equations 7-9. To produce 1 mole of aiming product, the mole of CO_3^{2-} ions formed is:

$$n_{\text{carbonate}} = 1\text{mol} \cdot n \cdot \frac{100\%}{\text{carbon efficiency}} - 1\text{mol} \cdot n \tag{23}$$

where n is the number of CO_2 molecules involved in the reaction. For the MEA setup, as shown in Supplementary Fig. 8d, the mole of CO_3^{2-} ions formed is:

$$n_{\text{carbonate}} = 1\text{mol} \cdot \frac{z}{2} \cdot \frac{100\%}{\text{FE}\%} \tag{24}$$

The energy consumption for electrolyte regeneration to produce 1 mole of aiming product is:

$$\Delta E_{\text{regeneration}} = n_{\text{carbonate}} \cdot 194.7\text{kJ} \cdot \text{mol}^{-1} \tag{25}$$

Supplementary Tables 2 and 3 summarize the energy consumption from each part to produce CO and ethylene, respectively, with different electrolyte media and setups.

Energy estimation of production of formic acid: Supplementary Fig. 10 shows the schemes of a sustainable system to produce formic acid based on a flow cell in acidic, near neutral, or alkaline media. An MEA based on AEM is not suited for this purpose since the formate ions formed on the cathode penetrate the AEM and can be oxidized at the anode before flowing out with the electrolyte solution, leading to significantly decreased carbon efficiency. A pressure swing distillation (PSD) unit[22] is used to separate formic acid from acidic aqueous solution. For systems in near neutral and alkaline media, an electrodialysis unit[23] is used to convert formate to formic acid before the PSD unit. The energy consumption of the PSD unit is about 265 kJ per mole of formic acid and water.[22] This part of energy is much higher than all the other parts

since water is the major part of the outlet solution from the cell. To have a higher energy efficiency, the concentration of formic acid in the solution should be as high as possible.

For CO_2 reduction in acidic medium, the formation of formic acid does not significantly change the electrolyte composition in the medium (namely K^+ ions, H^+ ions HSO_4^- ions and SO_4^{2-} ions). In the experiment in Supplementary Fig. 4, the concentration of formic acid in the electrolyte solution reached 1.21 M. In near neutral medium, formate ions are generated at the cathode and HCO^{3-} ions are consumed at the anode. The composition of the electrolyte solution changed gradually (from $KHCO_3$ to HCOOK). To keep a relatively constant composition of electrolytes, the concentration of formate as product should not be too high. For example, when a 0.5 M $KHCO_3$ solution is used, if only 0.05 M of formate is generated, the concentration variation of HCO_3^- ions exceeds 10%. In alkaline medium, the reaction between CO_2 and OH^- ions also led to a changing electrolyte composition. According to Supplementary Equations 7 and 8, the amount of CO_2 consumed by alkaline medium is about 7.5 times of that reduced to formate when the partial current density is 200 $mA \cdot cm^{-2}$. Therefore, to maintain a stable composition of the electrolyte solution, the concentration of formate in the outlet must be even lower than that in near neutral medium, leading to more energy consumption in the PSD step.

Additionally, when a near neutral or alkaline medium is used, AEM is used to separate anode from the flow media, but formate ions could penetrate AEM and be oxidized at the anode, leading to a further decrease of carbon efficiency.

Supplementary Note 2: Simulation Procedure

Supplementary Fig. 24 shows the governing equation and boundary conditions for the simulation of the cation effect on hydronium reduction. The transport of three solvated ionic species (K^+, H^+ and OTf^-) and the corresponding charge transfer were considered in the simulation. The Poisson-Nernst-Planck equations at steady state[24] are solved in the region between OHP and bulk electrolyte. These equations include the diffusion, migration and convection terms of each species:

$$\frac{\partial c_i}{\partial t} = -\frac{\partial J_{x,i}}{\partial x} = 0 \tag{26}$$

$$J_{x,i} = -D_i \frac{\mathrm{d}c_i}{\mathrm{d}x} - \frac{D_i c_i n_i F}{RT} \frac{\mathrm{d}\varphi}{\mathrm{d}x} + v_x c_i \tag{27}$$

where c_i is the concentration of species i (with i = K^+, H^+ and OTf^-), D_i is the diffusion coefficient of species i, n_i is the charge of species i, R is the ideal gas constant, T is the temperature, φ is the potential and v_x is the velocity of solution in x-direction. For a rotating disk electrode, the velocity in axial direction at different x-locations can be estimated as:[25]

$$v_x = -0.51x^2\sqrt{\frac{\omega^3}{\nu}} \tag{28}$$

where ω is the rotation speed (unit: rad·s^{-1}) of the disk electrode, ν is the kinematic viscosity of water.

The Poisson equation is used to calculate the potential change, given by:

$$\frac{\mathrm{d}}{\mathrm{d}x}\left(\varepsilon_0 \varepsilon_r \frac{\mathrm{d}\varphi}{\mathrm{d}x}\right) = -F\sum_i n_i c_i \tag{29}$$

where ε_0 is the permittivity of vacuum and ε_r is the relative permittivity of water.

The thickness of Stern layer (d_{Stern}) was assumed to be 0.4 nm.[26] The thickness of the region between OHP and bulk solution in simulation was assumed to be 100 μm, larger than the thickness of diffusion layer for hydronium ions (δ_{H}) estimated by:[25]

$$\delta_{\mathrm{H}} = 1.61 D_i^{1/3} \omega^{-1/2} \nu^{1/6} \tag{30}$$

Since hydronium ion has the largest diffusion coefficient, hydronium ion was used to estimate the thickness of the region for simulation. δ_{H} equals 52 μm as the rotating speed was 400 rpm, guaranteeing the region with concentration gradient was included in the domain for simulation.

The boundary conditions for the domain between OHP and bulk electrolyte consist of: At the right side (x = 100 μm), the concentration of each species equals to the bulk concentration of this species, and the potential equals to 0 V vs PZC. At the left side (x = 0), the flux of each species was given as:

$$J_{x,\mathrm{K^+}} = J_{x,\mathrm{OTf^-}} = 0 \tag{31}$$

$$J_{x,\mathrm{H^+}} = j_{\mathrm{H^+}}/F \tag{32}$$

where $j_{\mathrm{H^+}}$ is the current density of hydronium reduction. We assumed the current density of hydronium reduction showed proportional relations with hydronium concentration at OHP and exponential relations with the potential of cathode:

$$j_{\mathrm{H^+}} = -Ac_{\mathrm{H^+}}\exp(-\frac{\alpha F}{RT}\varphi_{\mathrm{cathode}}) \tag{33}$$

where α is the charge transfer coefficient and $\varphi_{\mathrm{cathode}}$ is the potential of cathode. Then, the current densities of hydronium reduction (j_0 and j_1) at two different conditions ($c^0_{\mathrm{H^+}}$, $\varphi^0_{\mathrm{cathode}}$ and $c^1_{\mathrm{H^+}}$, $\varphi^1_{\mathrm{cathode}}$) show the relationship as:

$$j_1 = j_0 \cdot \frac{c^1_{\mathrm{H^+}}}{c^0_{\mathrm{H^+}}} \cdot \exp(-\frac{\alpha F}{RT}\left(\varphi^1_{\mathrm{cathode}} - \varphi^0_{\mathrm{cathode}}\right)) \tag{34}$$

The experimental HER current density on a flat Au electrode at -0.4 V vs SHE in an acidic medium with pH = 1 was -1 mA·cm^{-2}.[27] The PZC of Au in an acidic medium with pH = 1 and containing weakly adsorbed anions (such as SO_4^{2-} and ClO_4^-) was 0.2 V vs SHE.[28] We assumed the PZC of Au in HOTf-KOTf solution with pH = 1 was also 0.2 V vs SHE. Therefore, we assigned $\varphi^0_{\mathrm{cathode}}$ = -0.6 V vs PZC, $c^0_{\mathrm{H^+}}$ = 0.1 M and j_0 = -

1 mA·cm^{-2} in Supplementary Equation 34. We assumed $\alpha = 0.5$. Then, the HER current density at a certain condition can be estimated as:

$$j_{\mathrm{H^+}} = -1\mathrm{mA}\cdot\mathrm{cm}^{-2}\cdot\frac{c_{\mathrm{H^+}}}{0.1\ \mathrm{M}}\cdot\exp\left(-\frac{0.5F}{RT}\left(\varphi_{\mathrm{cathode}}+0.6\ \mathrm{V}\right)\right) \quad (35)$$

To confirm that the accuracy of the above assignment did not affect the trends of simulated result, we also did the simulation with the $\varphi^0_{\mathrm{cathode}}$ value in Supplementary Equation 34 as -0.5 V and -0.7 V vs PZC. As shown in Supplementary Fig. 26, as the value of $\varphi^0_{\mathrm{cathode}}$ changed, the current density-potential curves in 0.1 M HOTf or 0.1 M HOTf + 0.4 M KOTf just shifted laterally and the shape of the curves did not change.

In Stern layer, the Poisson equation is given by:

$$\frac{\mathrm{d}}{\mathrm{d}x}\left(\varepsilon_0\varepsilon_r\frac{\mathrm{d}\varphi}{\mathrm{d}x}\right)=0 \quad (36)$$

The left boundary condition for Supplementary Equation 36 in Stern layer was:

$$\varphi_{x=-0.4\ \mathrm{nm}}=\varphi_{\mathrm{cathode}} \quad (37)$$

Neumann boundary condition was used for Supplementary Equation 29 at OHP ($x = 0$), namely:

$$\left(\varepsilon_0\varepsilon_r\frac{\mathrm{d}\varphi}{\mathrm{d}x}\right)_{x=0}=\varepsilon_0\varepsilon_r\frac{\varphi_{x=0}-\varphi_{\mathrm{cathode}}}{d_{\mathrm{Stern}}} \quad (38)$$

Simulation of interfacial pH

The pH profiles were explored from the PNP modeling. Hydronium ion reduction, OH^- generation from CO_2 reduction, the neutralization reaction between OH^- and hydronium ions, and dissociation of water molecules were subsequently included in the simulation. Supplementary Fig. 25 shows the governing equation and boundary conditions used in this simulation.

OH^- generation from water reduction was not included since this process occurred at more negative potential than the potential range in which we did the simulations. According to Fig. 4a, the onset potential of water reduction was around -1.25 V vs SHE,

corresponding to -1.45 V vs PZC. The most negative potential in our simulation was -1.26 V vs PZC. Supplementary Equation 26 is modified as:

$$\frac{\partial c_i}{\partial t} = -\frac{\partial J_{x,i}}{\partial x} + R_i = 0 \tag{39}$$

R_i represents the neutralization reaction between OH^- and hydronium ions and dissociation of water molecules:

$$R_{\mathrm{H^+}} = R_{\mathrm{OH^-}} = k_{w1} - k_{w2} c_{\mathrm{H^+}} c_{\mathrm{OH^-}} \tag{40}$$

where k_{w1} and k_{w2} are the rate constants of water dissociation and H^+-OH^- neutralization, respectively. For K^+ and OTf^- ions, $R_i = 0$. At $x = 0$, the flux of OH^- ions is:

$$J_{x,\mathrm{OH^-}} = -j_{\mathrm{CO_2}}/F \tag{41}$$

where j_{CO2} is the current density of CO_2 reduction, corresponding to OH^- generation in our case. Since on Au surface, the rate determining step of CO_2 reduction is CO_2 adsorption/electronation, the reaction rate is independent of local pH.[29] We assume j_{CO2} shows proportional relations with CO_2 concentration and exponential relations with the potential of cathode:

$$j_{\mathrm{CO_2}} = -A c_{\mathrm{CO_2}} \exp\left(-\frac{\alpha F}{RT}\varphi_{\mathrm{cathode}}\right) \tag{42}$$

Since a gas diffusion electrode is used for the CO_2 reduction, the current density of CO_2 reduction is generated at the triple phase interface (i.e. catalyst-gas-electrolyte interface) and in the adjacent thin liquid layer inside the pores (i.e.at the catalyst-electrolyte phase interface in the liquid). Additionally, the dissolved CO_2 in the liquid film is assumed to be maintained at equilibrium with the gas phase CO_2 in the pores over a wide potential range. Therefore, we assume c_{CO2} at the reaction interface is constant at different potentials. Supplementary Equation 42 is fit according to the partial current density of CO_2 reduction to CO on Au/C catalyst from -0.71 V to -1.01 V vs RHE (-1.01 V to -1.27 V vs PZC) in Fig. 1e. The fitting result is:

$$j_{\mathrm{CO_2}}(\mathrm{mA \cdot cm^{-2}}) = -10\text{^}(-9.83\varphi_{\mathrm{cathode}}(\mathrm{V\ vs\ PZC}) - 10.16) \tag{43}$$

The overall reduction current density is the sum of current densities of hydronium reduction and CO_2 reduction (namely OH^- production):

$$j = j_{H^+} + j_{CO_2} \quad (44)$$

The reaction between CO_2 and OH^- ions ($CO_2 + OH^- \rightarrow HCO_3^-$) was not considered in the simulation because the consumption rate of OH^- in this reaction is negligible compared to the formation rate of OH^- from CO_2 reduction. We take the simulation in 0.1 M HOTf + 0.4 M KOTf at -1.26 V vs PZC as an example. At this condition, the current density of CO_2 reduction was 170 $mA \cdot cm^{-2}$ (Fig. 6d), corresponding to a formation rate of OH^- of 1.76×10^{-6} $mol \cdot s^{-1} \cdot cm^{-2}$. The consuming rate of OH^- by the reaction with CO_2 can be estimated by Supplementary Equation 7. Since $[OH^-]$ varies at different position, we take the maximum value of $[OH^-]$ into Supplementary Equation 7 and we can get an upper limit of the consumption rate of OH^-. The maximum pH value was 6.3 (Fig. 6a), corresponding to $[OH^-] = 2\times10^{-8}$ M. Therefore, the consumption rate of OH^- is smaller than 1×10^{-9} $mol \cdot s^{-1} \cdot cm^{-2}$, negligible compared with the formation rate of OH^- (1.76×10^{-6} $mol \cdot s^{-1} \cdot cm^{-2}$). Therefore, the reaction between CO_2 and OH^- can be neglected in the simulation of interfacial pH.

Supplementary Fig. 21a and 21b show the overall reduction current density and pH at OHP at different potential with 0.1 M HOTf, 0.1 M HOTf + 0.1 M KOTf and 0.1 M HOTf + 0.4 M KOTf. In K^+-free medium, the simulation was done from -0.5 V to -0.7 V. In K^+-containing media, the simulation was done from -0.5 V to -1.26 V. Simulation at more negative potential led to a convergence problem.

Supplementary Fig. 21c compares the simulated pH profiles in 0.1 M HOTf + 0.4 M KOTf at -1.26 V vs PZC with and without the consideration of OH^- generation from CO_2 reduction at the cathode in the simulation. For the simulation without the consideration of OH^- generation from CO_2 reduction, j_{CO2} was set to 0, and the homogeneous reaction between hydronium ions and OH^- ions and the dissociation of water molecules were considered.

Numerical details:

Supplementary Table 4 summarizes the values of the various parameters in the model. A mesh independence study was conducted, resulting in the choice of a uniformly distributed mesh with mesh element size of 0.66×10^{-9} m. A smaller mesh size results in mesh elements smaller than the size of the individual ions. A further decrease in the mesh size resulted in a change in current density, electrolyte potential and concentrations of H^+ and OTf^- of less than 3%. The coupled equations were solved with a commercial solver (COMSOL 5.5) utilizing a MUMPS solver with a non-linear automatic Newton method. The solution was converged when a relative tolerance of 0.001 was reached. Further increasing the relative tolerance resulted in a difference in the results of less than 1%.

For the simulations without the CO_2 reduction and equilibrium reactions, a stationary solver was used. Typically, 10 to 20 iterations were needed for convergence. For the simulations that incorporated the pH distribution near the cathode during the CO_2 reduction and the equilibrium reactions, a two-steps solution procedure was used. Firstly, a time dependent solver with a 1 micro second time step, running up to 10 micro seconds of reaction, was used. The result of this time dependent study was used as initial conditions of a stationary solver. In the stationary solver, two segregated steps were considered: one included the variables concentration of K^+, H^+ and OTF^- as well as the liquid potential, and the other included the concentration of OH^-.

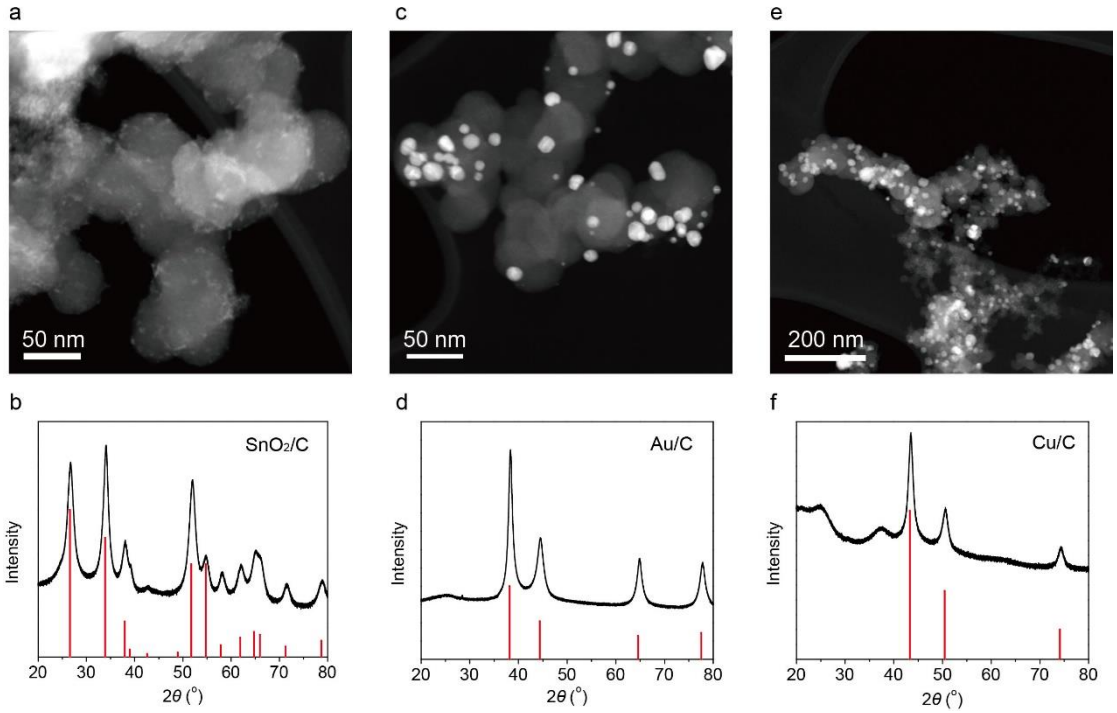

Supplementary Fig. 1 | Characterization of catalysts. (a, c, e) HAADF-STEM images and (b, d, f) PXRD patterns of (a, b) SnO_2/C, (c, d) Au/C and (e, f) Cu/C. The red vertical lines in (b), (d) and (f) are standard diffraction peaks of tetragonal SnO_2 (JCPDS no. 05-0467), face-center-cubic Au (JCPDS no. 04-0784) and face-center-cubic Cu (JCPDS no. 04-0836), respectively.

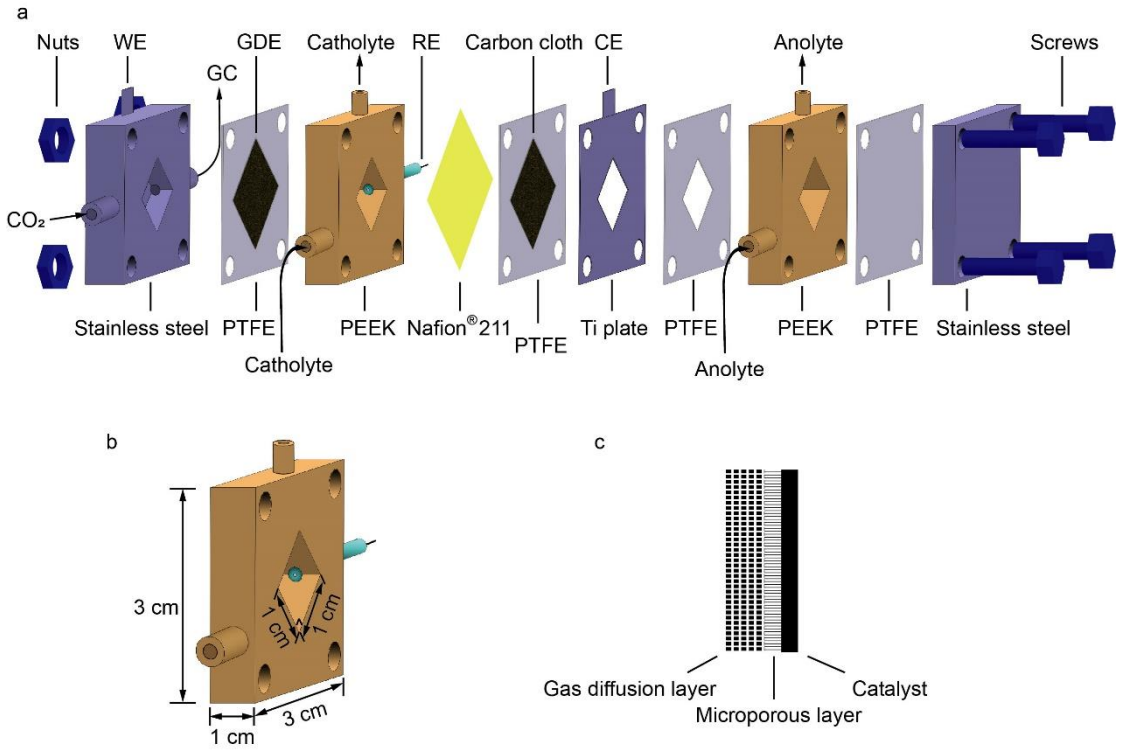

Supplementary Fig. 2 | Scheme of the three-electrode flow cell. (a) Structure of the whole assembly. The material for each part is indicated. WE: working electrode; RE: reference electrode; CE: counter electrode; PTFE: polytetrafluoroethylene; PEEK: polyether ether ketone. (b) Dimensions of the chamber of electrolyte solutions. (c) Scheme of the working electrode. The catalyst was sprayed onto the microporous layer of GDE (CeTech, W1S1009).

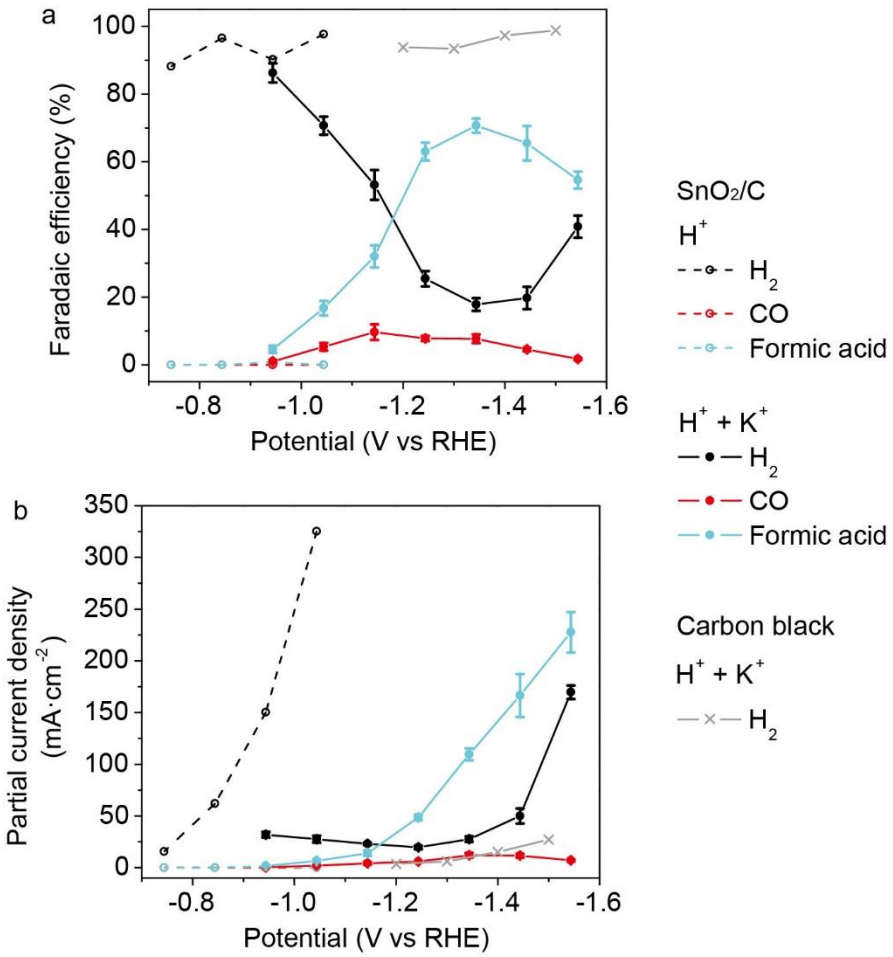

Supplementary Fig. 3 | Comparison of CO_2 reduction in acidic medium with and without K^+ ions. (a) Faradaic efficiency and (b) partial current density of H_2 (black), CO (red) and formic acid (light blue). The catalyst was SnO_2/C. The electrolyte was 0.1 M HOTf (dashed lines) or 0.1 M HOTf + 0.4 M KOTf (solid lines). Faradaic efficiency and partial current density of H_2 of Vulcan XC-72R in 0.1 M HOTf + 0.4 M KOTf was also shown as grey plots. Error bars were standard deviations based on tests of 3 individual working electrodes.

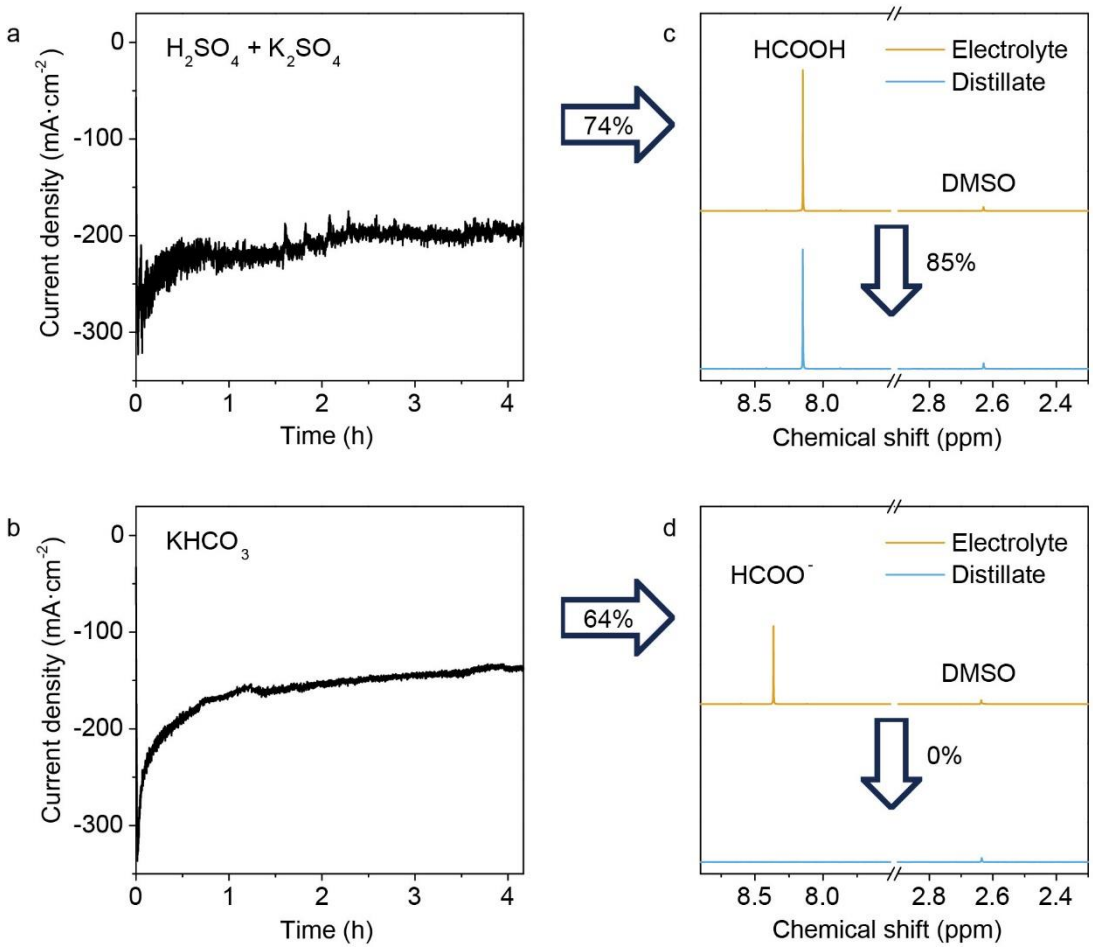

Supplementary Fig. 4 | Analysis and separation of solution-phase product of CO_2 reduction in acidic (0.1 M H_2SO_4 + 0.4 M K_2SO_4) and near neutral (0.8 M $KHCO_3$) media with SnO_2/C catalyst. (a, b) Chronoamperometry curves of SnO_2/C at -1.5 V vs SHE. (c, d) ^{1}H-NMR spectra of electrolyte solution after electrolysis (orange) and distillate of electrolyte solution (blue). DMSO was the internal standard. The Faradaic efficiency of formic acid and formate was 74% and 64%, respectively, and the recovery rates of distillation for formic acid and formate are 85% and 0%, respectively. The concentrations of formic acid in the electrolyte solution and the distillate were 1.21 M and 1.03 M, respectively.

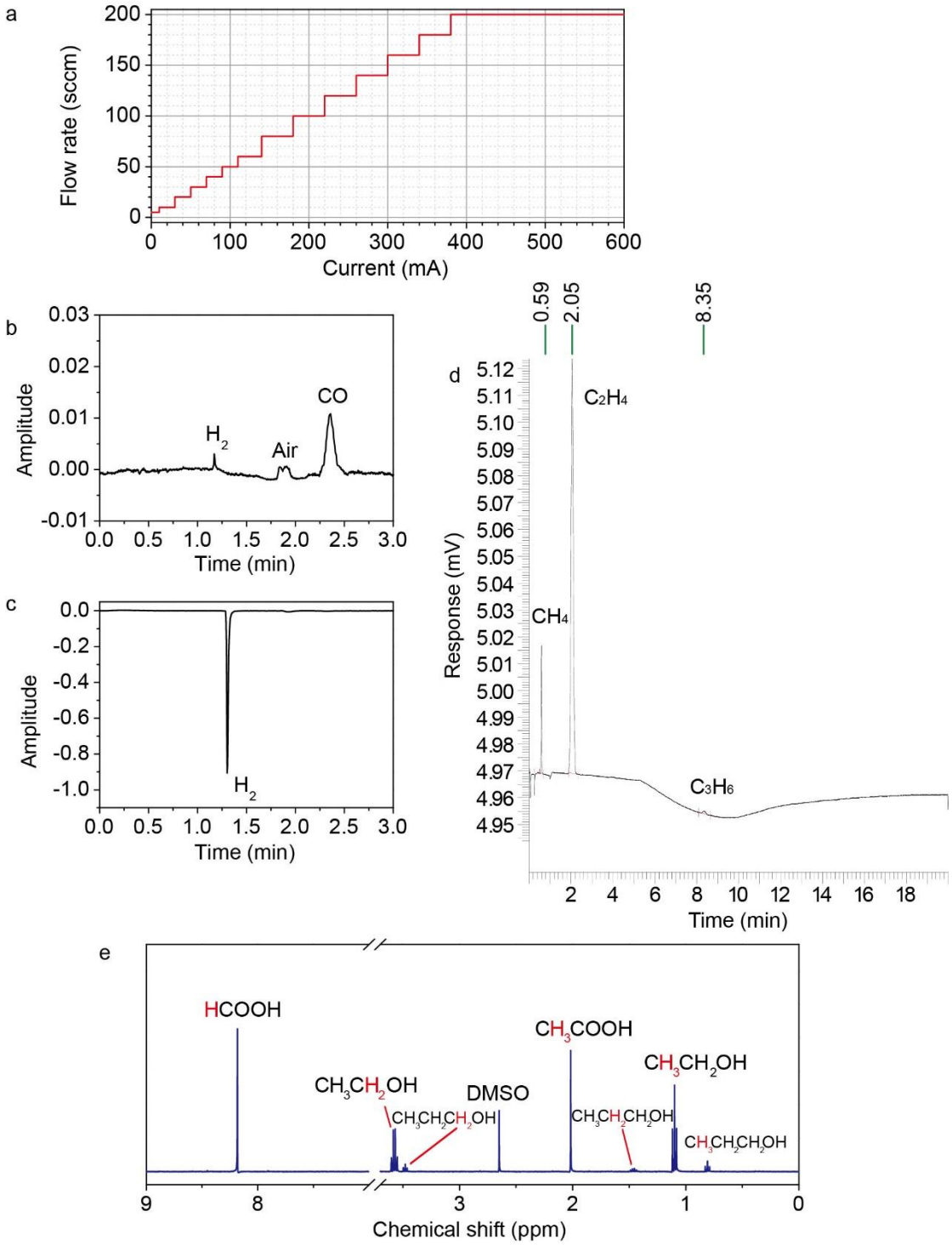

Supplementary Fig. 5 | Products of CO_2 reduction on Cu/C. (a) Tuning the flow rate of CO_2 according to the current of electrolysis. (b) GC-TCD curve with He as the carrier gas. (c) GC-TCD curve with Ar as the carrier gas. (d) GC-FID curve. (e) ^{1}H-NMR spectrum of catholyte solution after electrolysis. For ethanol and 1-propanol, the peaks corresponding to methyl group were used for quantification. Electrolyte: 0.1 M H_2SO_4 + 0.4 M K_2SO_4. Chronoamperometry test at -1.41 V vs RHE for 1800 s.

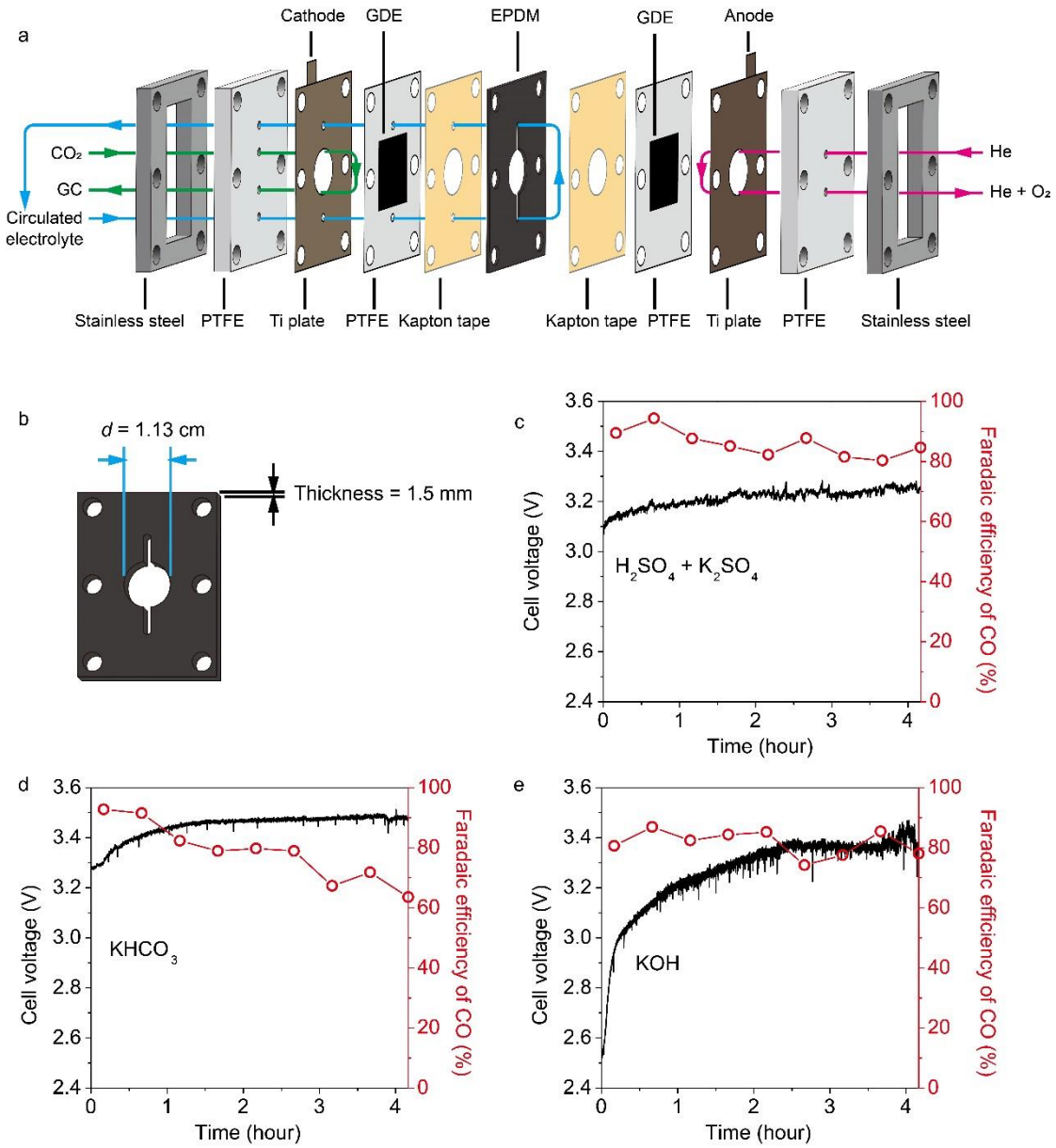

Supplementary Fig. 6 | Electrolysis with two-electrode flow cell. Scheme of the two-electrode flow cell: (a) structure of the whole assembly and (b) dimensions of the chamber for the electrolyte solutions. CO_2 electroreduction on Au/C in the two-electrode cell with (c) 0.1 M H_2SO_4 + 0.4 M K_2SO_4, (d) 0.8 M $KHCO_3$, and (e) 0.8 M KOH as the electrolyte solutions. Black curves: cell voltage; red curves: Faradaic efficiency of CO.

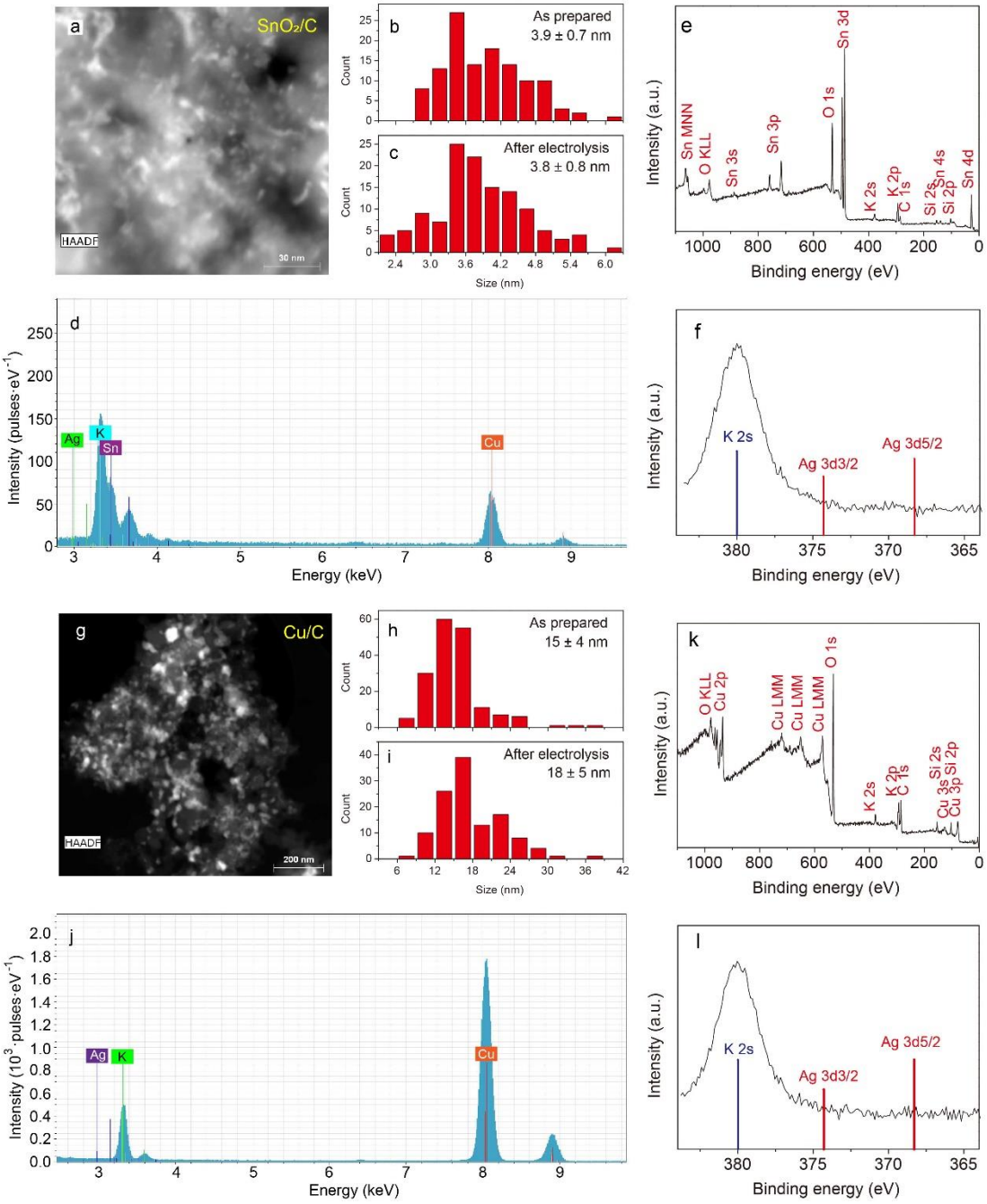

Supplementary Fig. 7 | Characterizations of SnO_2/C and Cu/C after electrolysis tests. SnO_2/C catalyst: (a) HAADF-STEM image after electrolysis; Size distribution of nanoparticles (b) before and (c) after electrolysis; (d) X-ray energy dispersive spectrum (EDS) after electrolysis; (e) survey and (f) Ag3d region high resolution X-ray photoelectron spectrum (XPS) after electrolysis. Cu/C catalyst: (g) HAADF-STEM image after electrolysis; Size distribution of nanoparticles (h) before and (i) after electrolysis; (j) X-ray energy dispersive spectrum (EDS) after electrolysis; (k) survey and (l) Ag3d region high resolution X-ray photoelectron spectrum (XPS) after electrolysis. Ag was not observed in EDS and XPS after electrolysis, indicating no contamination from the Ag/AgCl reference electrode.

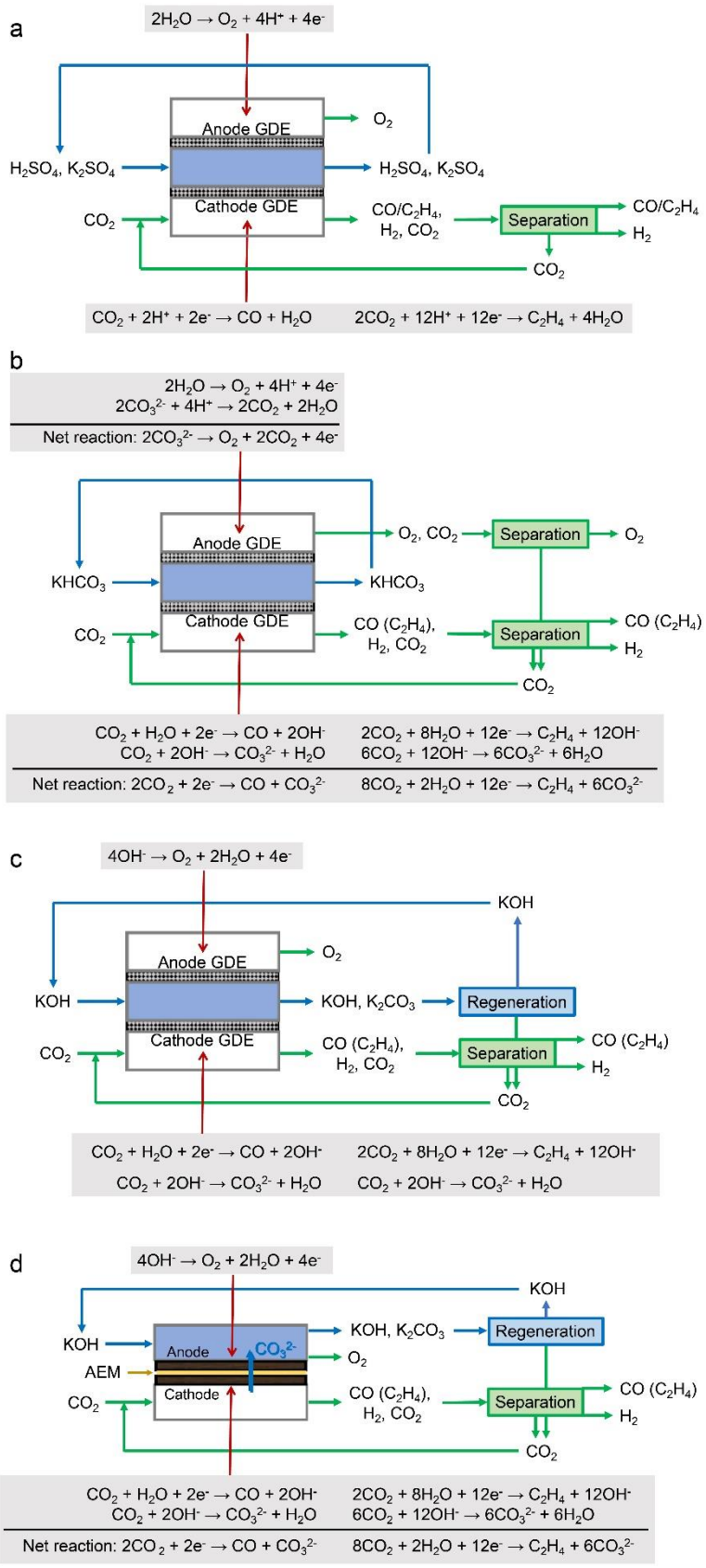

Supplementary Fig. 8 | Scheme of sustainable CO_2 reduction systems to produce CO or ethylene. (a) In acidic medium; (b) In near neutral medium; (c) In alkaline medium; (d) MEA setup with anion exchange membrane (AEM).

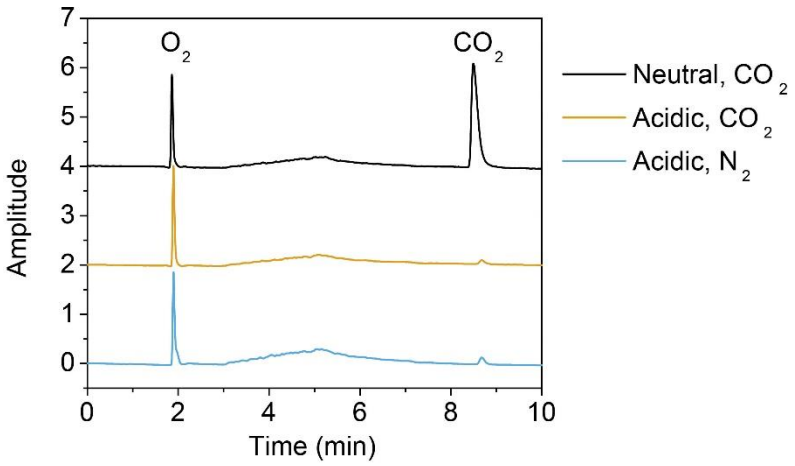

Supplementary Fig. 9 | GC curves of gas generated at the anode compartment. Au/C and IrO_2 were used as catalysts for cathode and anode, respectively. Helium was supplied behind anode. Black curve: near neutral medium (0.8 M $KHCO_3$) was used and CO_2 was supplied behind the cathode. Orange curve: acidic medium (0.1 M H_2SO_4 + 0.4 M K_2SO_4) was used and CO_2 was supplied behind the cathode. Blue curve: acidic medium was used and N_2 was supplied behind the cathode. GC samples were taken after electrolysis at 200 $mA \cdot cm^{-2}$ for 3 h to ensure the system reached a steady state. The small peaks of CO_2 from acidic medium were due to the oxidation of carbon cloth.

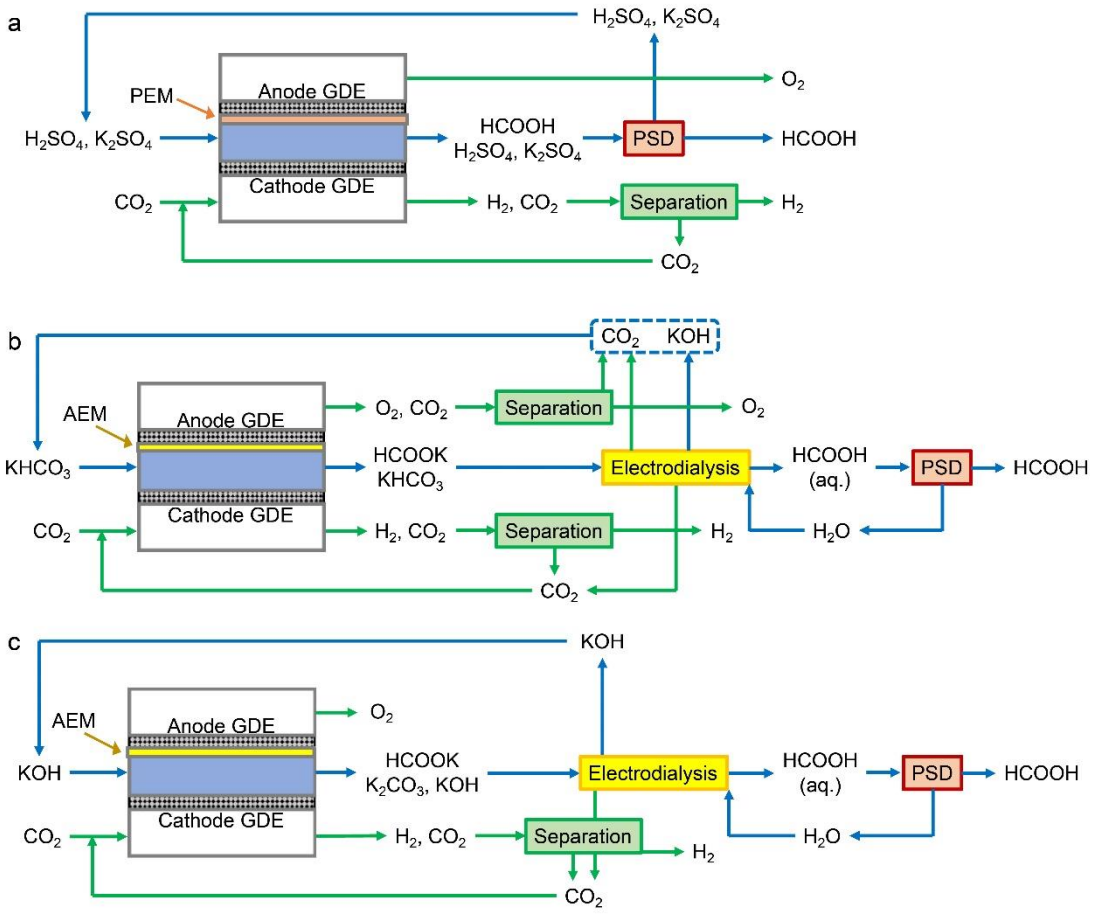

Supplementary Fig. 10 | Scheme of system with a flow cell for sustainable CO_2 reduction to produce formic acid. (a) acidic medium; (b) near neutral medium; (c) alkaline medium.

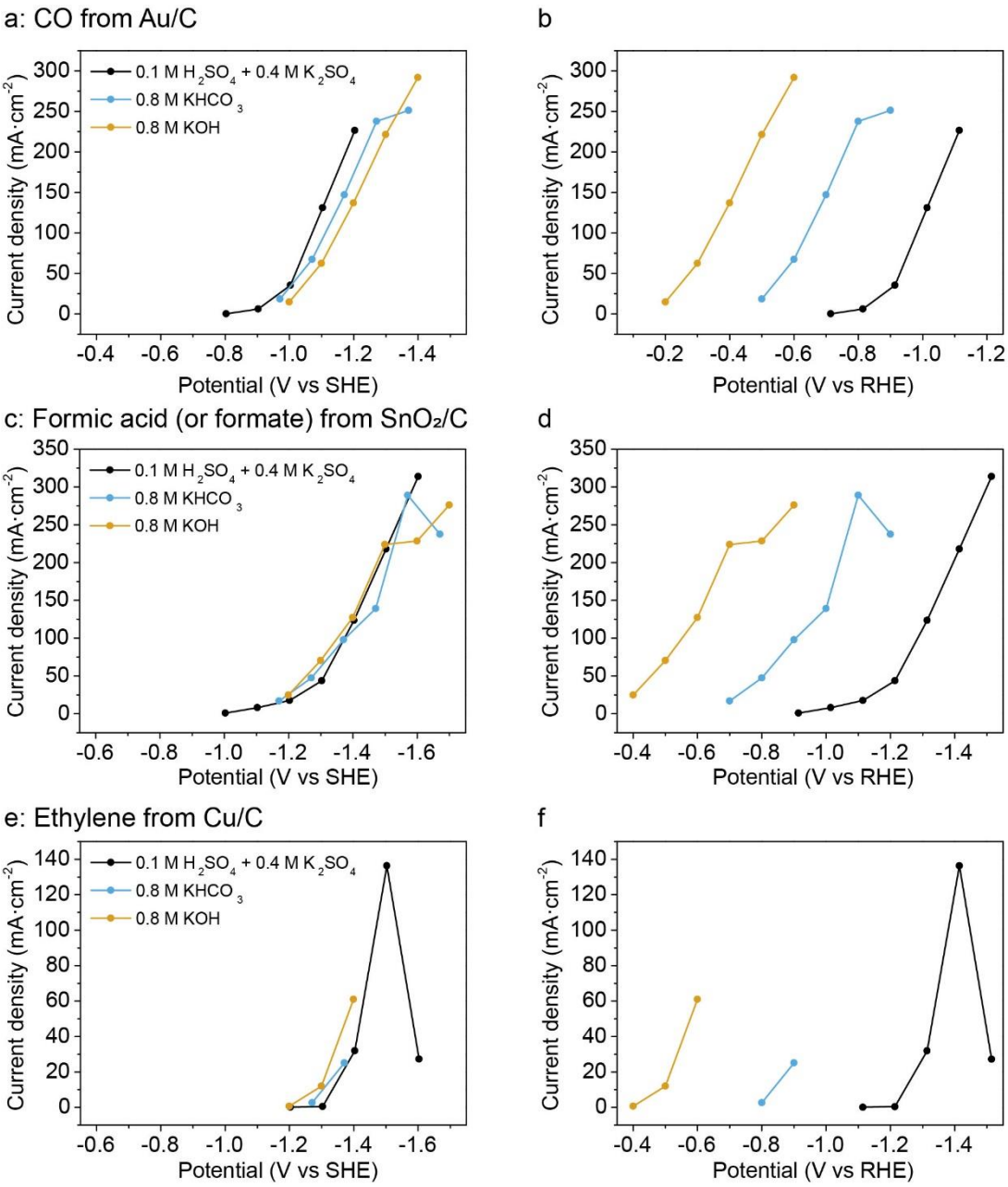

Supplementary Fig. 11 | Plots of partial current density of CO_2 reduction on potential vs SHE and RHE. (a, b) CO formation from Au/C catalyst. (c, d) Formic acid or formate formation from SnO_2/C catalyst. (e, f) Ethylene formation from Cu/C catalyst. (a, c, e) Plots based on SHE. (b, d, f) Plots based on RHE. Electrolyte: (black) 0.1 M H_2SO_4 + 0.4 M K_2SO_4; (blue) 0.8 M $KHCO_3$; (orange) 0.8 M KOH.

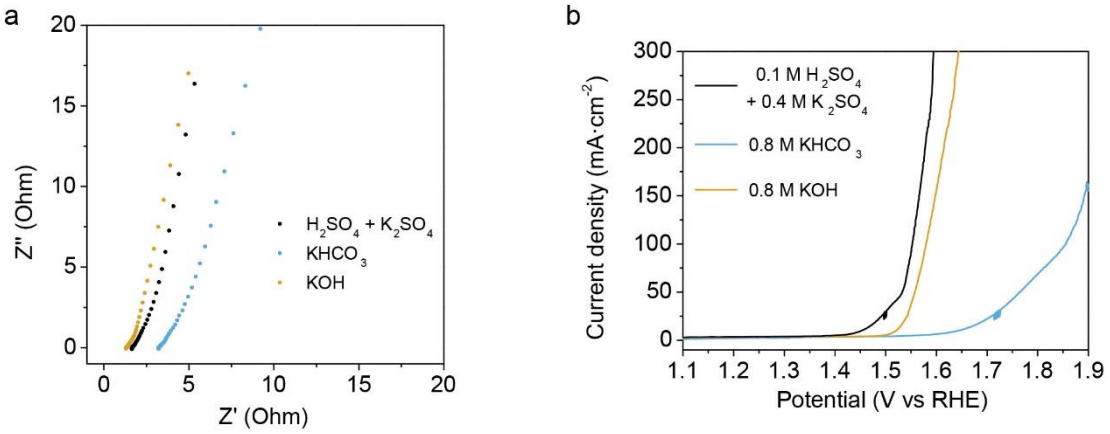

Supplementary Fig. 12 | Resistance and OER overpotential in different media. (a) Nyquest plots at open circuit potential. The real part of high-frequency-limiting impedance is regarded as the resistance of electrolyte solution. Thus, the resistances of 0.1 M H_2SO_4 + 0.4 M K_2SO_4, 0.8 M $KHCO_3$, and 0.8 M KOH, were 1.65 Ω, 3.19 Ω and 1.30 Ω, respectively. (b) LSV curves of IrO_2 anode. The sweeping rate was 20 $mV \cdot s^{-1}$. Electrolyte solutions: (black) 0.1 M H_2SO_4 + 0.4 M K_2SO_4; (blue) 0.8 M $KHCO_3$; (orange) 0.8 M KOH.

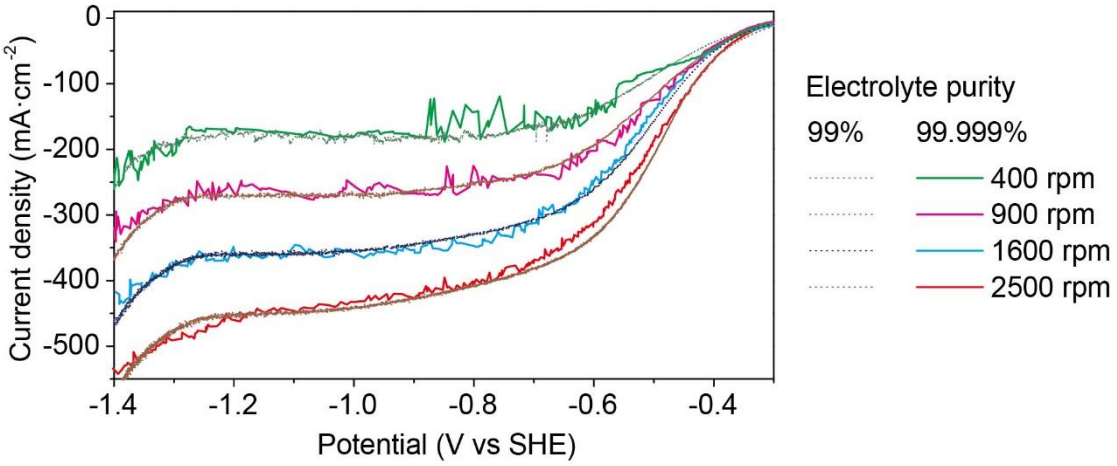

Supplementary Fig. 13 | Comparison of LSV curves collected in electrolytes with different purity. LSV curves of Au RDE in N_2 saturated solutions of 0.1 M HOTf + 0.4 M KOTf. Dotted curves were collected in electrolyte prepared by HOTf (99%) and KOTf (99%). Solid curves were collected in electrolyte prepared by partially neutralizing HOTf (99%) by electronic grade KOH (99.999%, Aladdin).

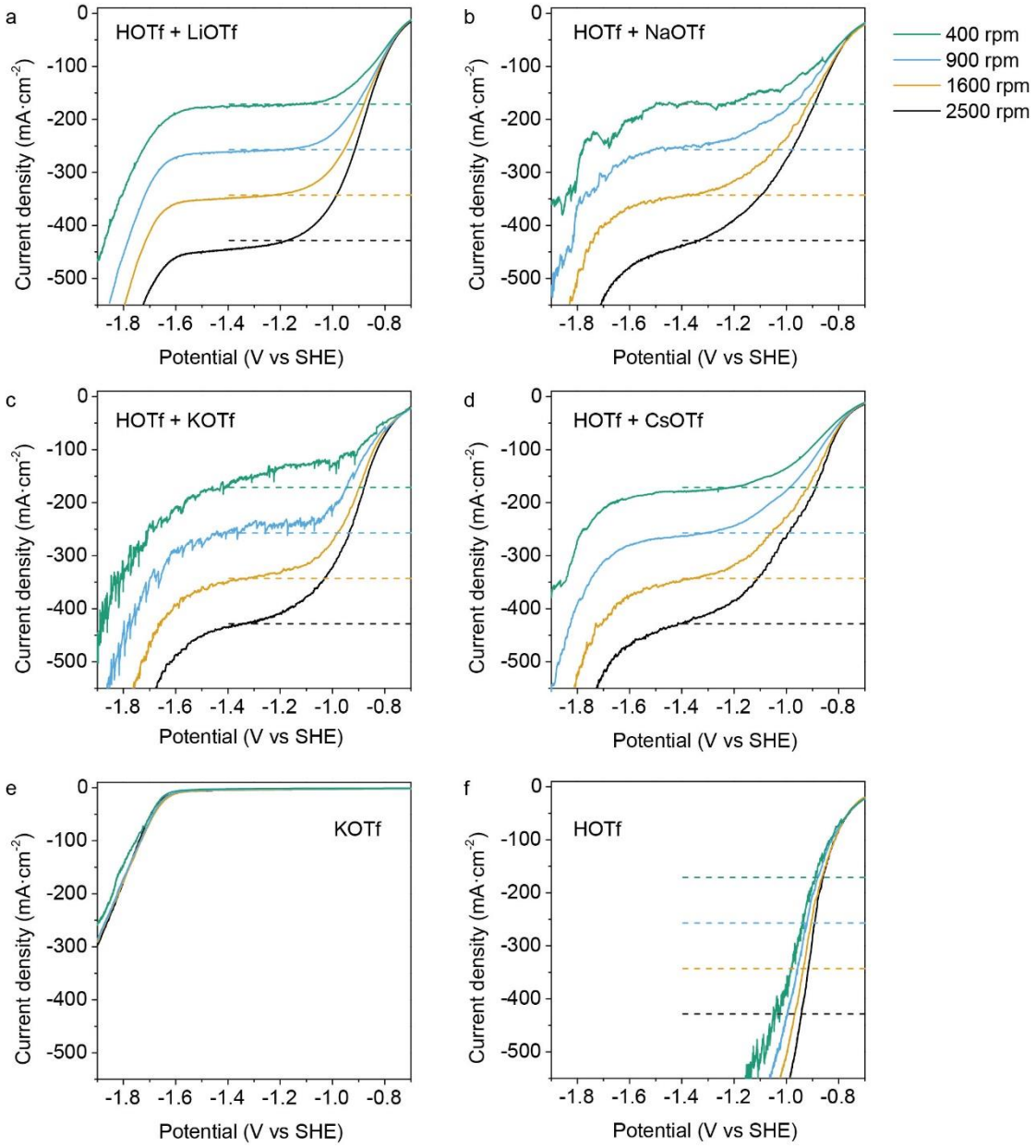

Supplementary Fig. 14 | LSV curves of HER by SnO_2/C on RDE in different electrolyte solutions. (a) 0.1 M HOTf + 0.4 M LiOTf. (b) 0.1 M HOTf + 0.4 M NaOTf. (c) 0.1 M HOTf + 0.4 M KOTf. (d) 0.1 M HOTf + 0.4 M CsOTf. (e) 0.4 M KOTf. (f) 0.1 M HOTf. All electrolyte solutions were saturated with N_2. Rotating speed: 400 rpm (green), 900 rpm (blue), 1600 rpm (orange) and 2500 rpm (black). The horizontal dashed lines of each color indicate the limiting diffusion current densities of the reduction of hydronium ions calculated according to Levich equation at the corresponding rotating speeds.

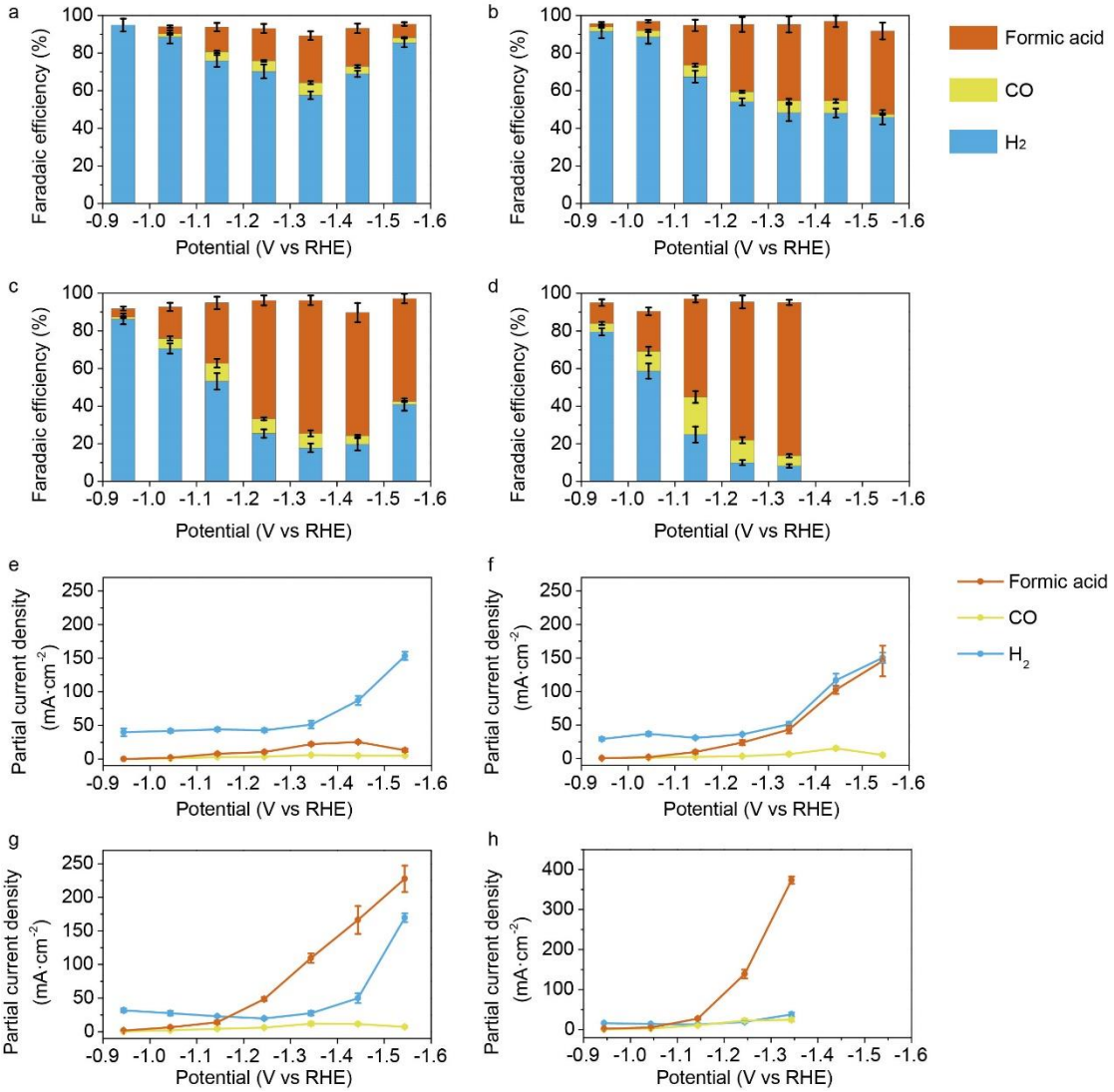

Supplementary Fig. 15 | CO_2 reduction catalyzed by SnO_2/C in acidic medium containing different alkali ions. (a-d) Faradaic efficiency and (e-h) partial current densities of different products. Electrolyte: (a, e) 0.1 M HOTf + 0.4 M LiOTf. (b, f) 0.1 M HOTf + 0.4 M NaOTf. (c, g) 0.1 M HOTf + 0.4 M KOTf. (d, h) 0.1 M HOTf + 0.4 M CsOTf. Error bars were standard deviations based on tests of 3 individual working electrodes.

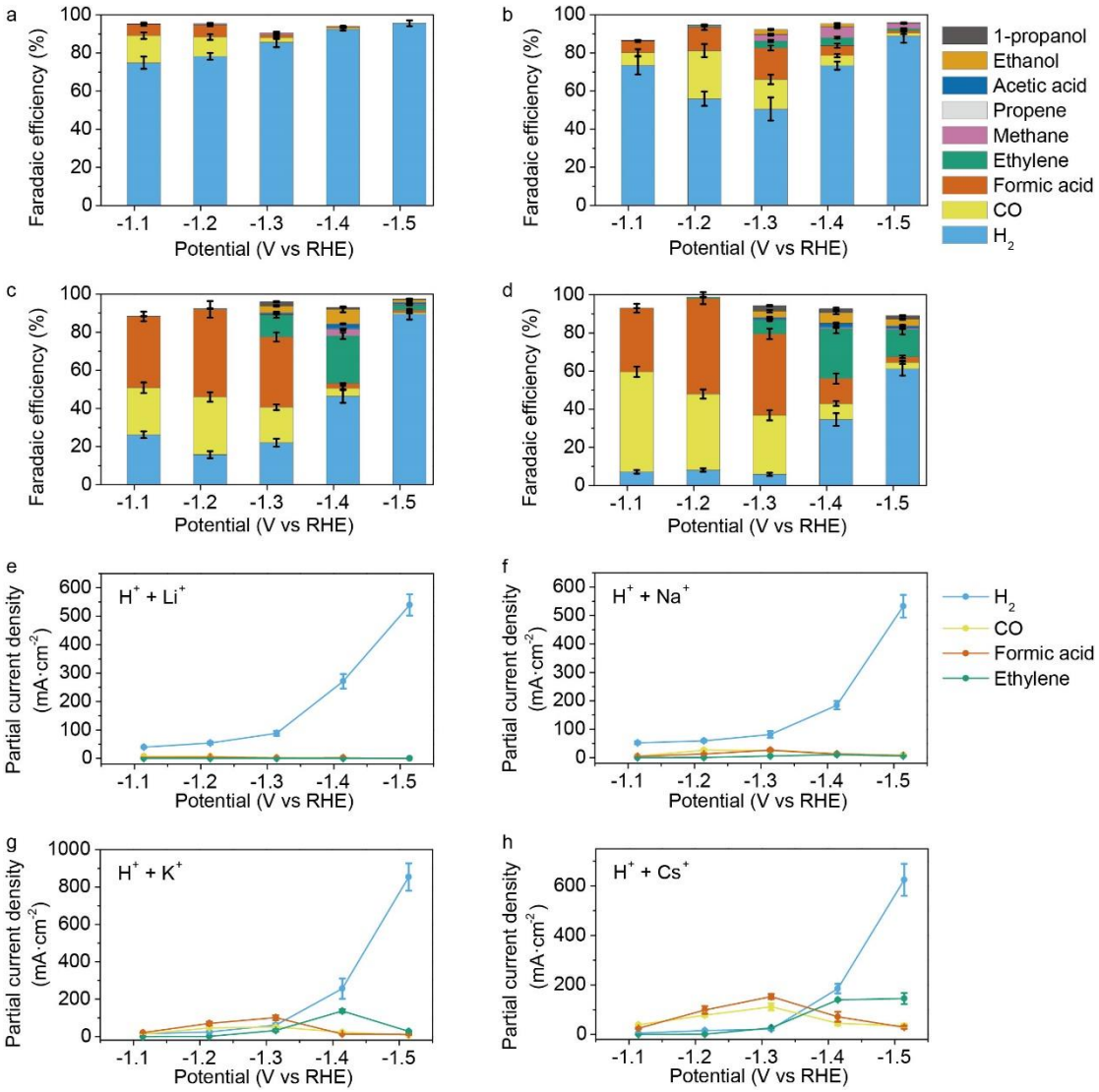

Supplementary Fig. 16 | CO_2 reduction catalyzed by Cu/C in acidic medium containing different alkali ions. (a-d) Faradaic efficiency and (e-h) partial current density of different products. Electrolyte: (a, e) 0.1 M H_2SO_4 + 0.4 M Li_2SO_4. (b, f) 0.1 M H_2SO_4 + 0.4 M Na_2SO_4. (c, g) 0.1 M H_2SO_4 + 0.4 M K_2SO_4. (d, h) 0.1 M H_2SO_4 + 0.4 M Cs_2SO_4. Error bars were standard deviations based on tests of 3 individual working electrodes.

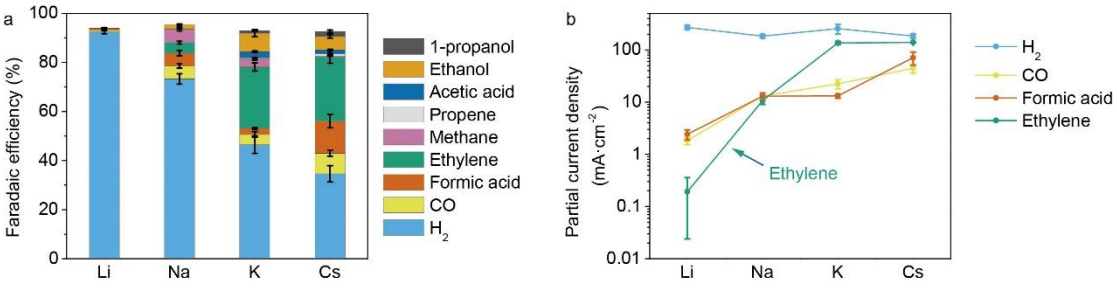

Supplementary Fig. 17 | Cation effects for CO_2 reduction on the Cu/C catalyst. (a) Faradaic efficiency and (b) partial current densities in electrolyte solutions with different alkali ions at -1.41 V vs RHE. The electrolyte was 0.1 M H_2SO_4 + 0.4 M M_2SO_4 (M = Li, Na, K, Cs). Error bars were standard deviations based on tests of 3 individual working electrodes.

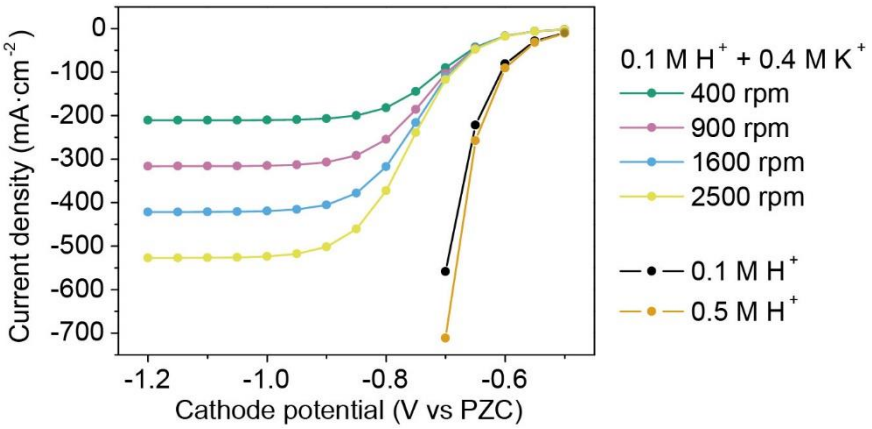

Supplementary Fig. 18 | Simulated HER current density of Au electrode based on PNP model. 0.1 M HOTf + 0.4 M KOTf (green, light pink, blue and yellow curves were simulated with the rotating speed of 400, 900, 1600, and 2500 rpm, respectively), 0.1 M HOTf (black, 400 rpm) and 0.5 M HOTf (orange, 400 rpm). It is noteworthy that the plateau current density in 0.1 M HOTf + 0.4 M KOTf is 25% higher than the limiting diffusing current density of hydronium reduction at the corresponding rotating speed based on Levich equation. While in the experimental result in Fig. 4a, the plateau current density was about 6% higher than the limiting diffusion current density. This difference was ascribed to neglecting the steric effect of cations in our PNP model. If the steric effect was considered, the repulsion from K^+ ions to H^+ ions near OHP is expected to be stronger, leading to lower concentration of H^+ near cathode and lower HER current density, closer to the HER current density in our experiment observation.

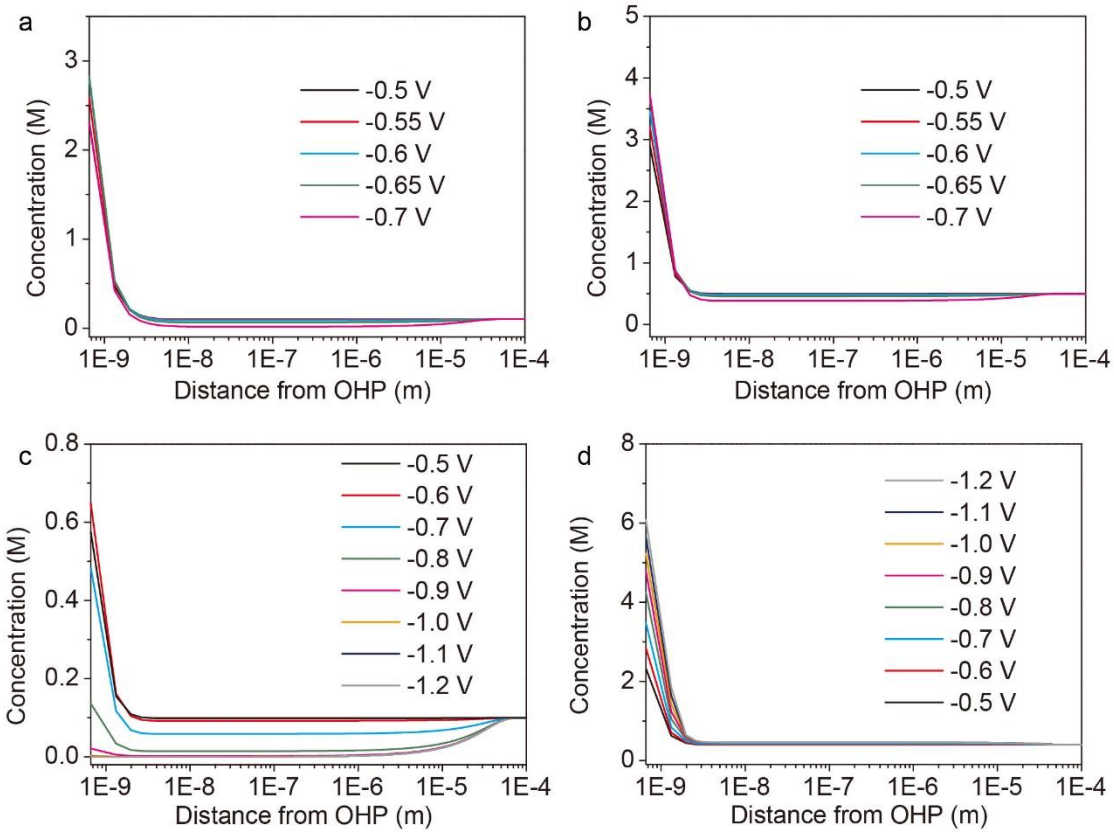

Supplementary Fig. 19 | Concentration profiles of H^+ and K^+ obtained from simulation based on PNP model. (a) Profiles of H^+ in 0.1 M HOTf. (b) Profiles of H^+ in 0.5 M HOTf. (c) Profiles of H^+ in 0.1 M HOTf + 0.4 M KOTf. (d) Profiles of K^+ in 0.1 M HOTf + 0.4 M KOTf. The rotating speed of RDE was 400 rpm. The potentials of cathode are vs PZC.

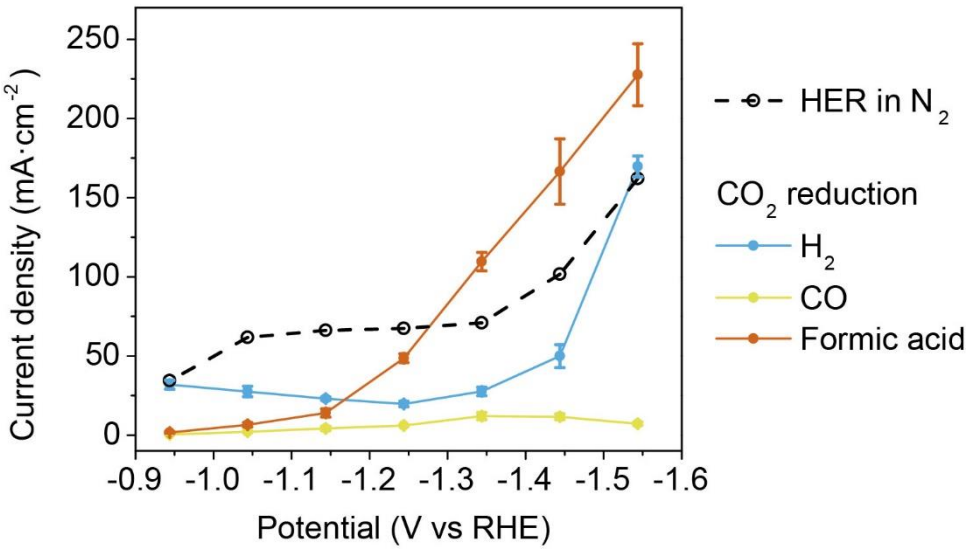

Supplementary Fig. 20 | Comparison of HER in an atmosphere of N_2 and CO_2. The catalyst was SnO_2/C and the electrolyte was 0.1 M HOTf + 0.4 M KOTf. The black dashed line shows the current density in N_2. The solid lines show the partial current densities of H_2 (blue), CO (yellow) and formic acid (orange) in CO_2. In N_2, a plateau of current density of about 65 $mA{\cdot}cm^{-2}$ was observed, corresponding to the diffusion limited current density for hydronium reduction. The partial current density of formic acid could be much higher than 65 $mA{\cdot}cm^{-2}$, indicating water as the proton source for CO_2 reduction. Consequently OH^- ions were generated during CO_2 reduction, similar to the reactions in near neutral and alkaline media. The OH^- reacted with hydronium ions, decreasing the HER current density compared to the reaction in N_2. Error bars were standard deviations based on tests of 3 individual working electrodes.

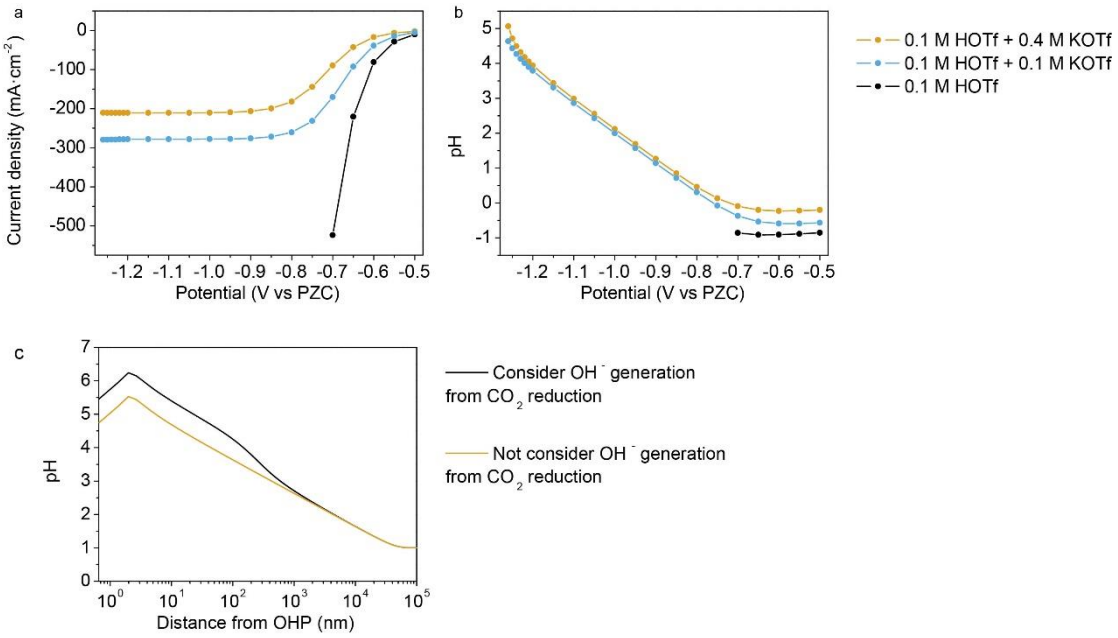

Supplementary Fig. 21 | Simulation results considering OH^- generation. (a) Overall reduction current density and (b) pH at OHP in 0.1 M HOTf + 0.4 M KOTf (orange), 0.1 M HOTf + 0.1 M KOTf (blue) and 0.1 M HOTf (black) at different potentials. The rotating speed was 400 rpm. In K^+-free medium, the simulation was done from -0.5 V to -0.7 V. In K^+-containing media, the simulation was done from -0.5 V to -1.26 V. Simulation at more negative potential led to convergence problems. Higher concentration of alkali cations led to more suppression of hydronium reduction. The local pH value (at OHP) at which the current density reached the plateau were similar in 0.1 M HOTf + 0.4 M KOTf and in 0.1 M HOTf + 0.1 M KOTf. In 0.1 M HOTf + 0.4 M KOTf, a current density of -211 mA·cm^{-2} (at -1.26 V) led to a significant increase of pH at OHP (pH = 5.1). In 0.1 M HOTf, a similar current density of -221 mA·cm^{-2} (at -0.65 V) did not lead to pH increase at OHP (pH = -0.9). Therefore, alkali cations are indispensable for the local pH increase in acidic media. (c) pH profiles in 0.1 M HOTf + 0.4 M KOTf at -1.26 V with (black curve) and without (orange curve) the consideration of OH^- generation from CO_2 reduction at the cathode in the simulation.

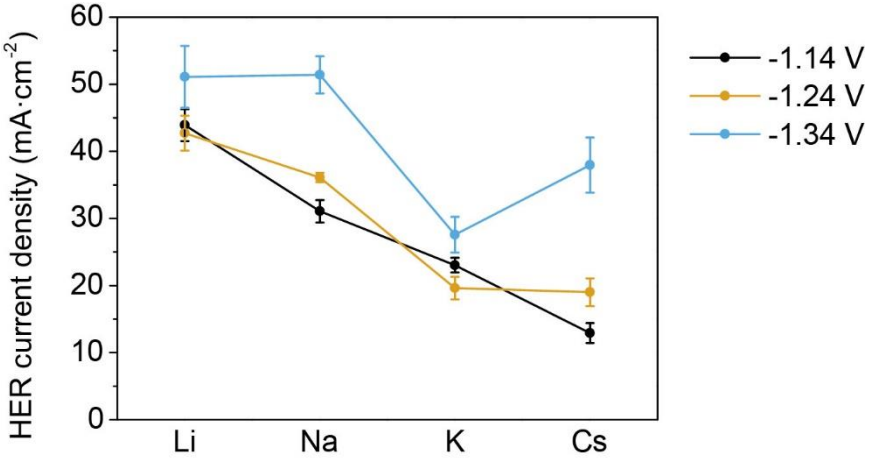

Supplementary Fig. 22 | Cation effect on HER in CO_2 atmosphere. HER current densities in a flow cell in 0.1 M HOTf + 0.4 M KOTf medium and fed with CO_2 gas. The catalyst was SnO_2/C. The potential of cathode was -1.14 V vs RHE (black), -1.24 V vs RHE (orange) and -1.34 V vs RHE (blue). At -1.14 V and -1.24 V, the HER current density showed a decreasing trend from Li to Cs. We attribute this trend to the suppression of hydronium reduction due to CO_2 reduction. The CO_2 reduction was promoted most in a Cs^+-containing medium. Thus, the highest amount of OH^- ions were generated in this case, which neutralized the highest amounts of hydronium ions, leading to the lowest current density of hydronium reduction. At -1.34 V, this trend was disrupted because the reduction of water molecules also contributed to HER at this potential. Water reduction was not suppressed by OH^- ions. Error bars were standard deviations based on tests of 3 individual working electrodes.

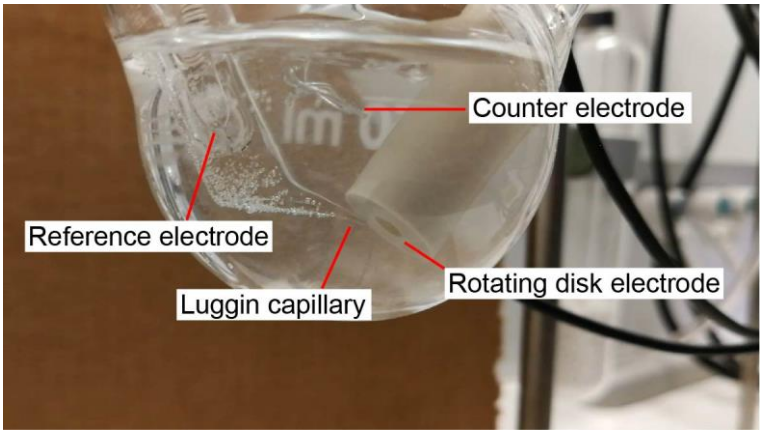

Supplementary Fig. 23 | Set up for RDE experiment. Au RDE in 0.1 M HOTf + 0.4 M KOTf. The current density was -200 $mA \cdot cm^{-2}$ and the rotating speed was 1600 rpm.

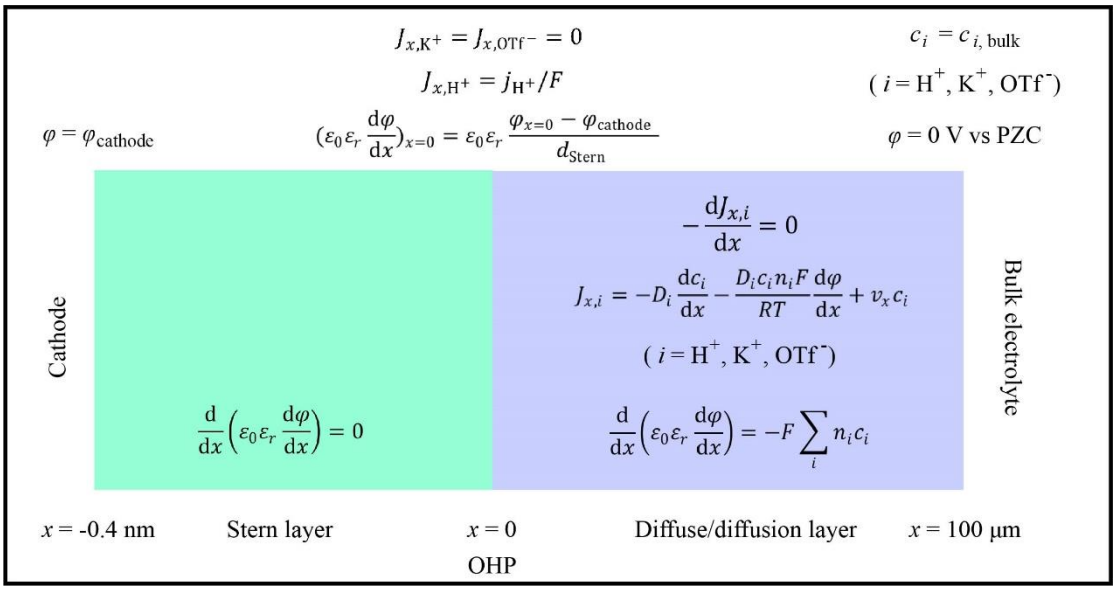

Supplementary Fig. 24 | Governing equations and boundary conditions used for the 1-dimensional simulation. From left to right: the cathode, the Stern layer, the diffuse/diffusion layer, and the bulk electrolyte region. OHP is used as origin (x=0).

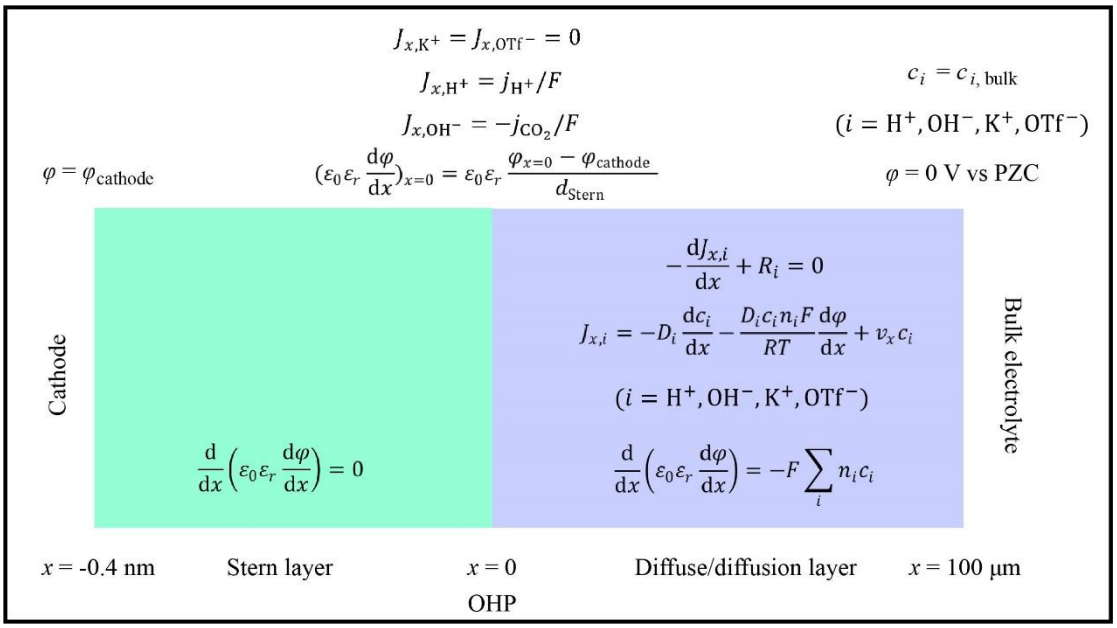

Supplementary Fig. 25 | Governing equations and boundary conditions used for the simulation of interfacial pH.

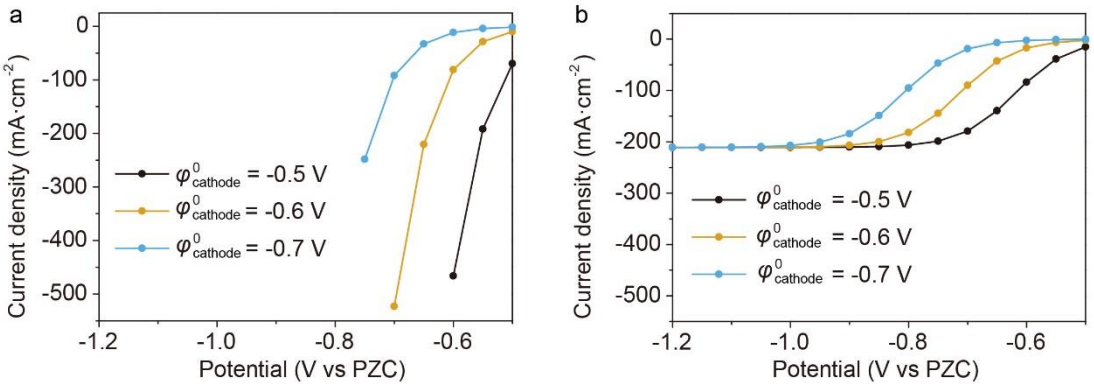

Supplementary Fig. 26 | Simulated HER current density-potential curves with different kinetic parameters. (A) In 0.1 M HOTf. (B) In 0.1 M HOTf + 0.4 M KOTf. The $\varphi^0_{\mathrm{cathode}}$ value in Supplementary Equation 34 was set to -0.5 V (black curves), -0.6 V (orange curves) and -0.7 V (blue curves), respectively.

Supplementary Table 1 | Concentration of Sn and Cu element in electrolyte solution and dissolving ratio of Sn and Cu after electrolysis (chronopotentiometry test at -200 $mA \cdot cm^{-2}$ for 15000 s).

Electrolyte	SnO_2/C catalyst		Cu/C catalyst	
	c(Sn) / $mg \cdot L^{-1}$	Dissolving ratio	*c*(Cu) / $mg \cdot L^{-1}$	Dissolving ratio
0.1 M HOTf + 0.4 M KOTf	1.08	1.70%	0.14	0.27%
0.8 M $KHCO_3$	0.73	1.15%	0.06	0.12%
0.8 M KOH	0.30	0.47%	0.01	0.02%

Supplementary Table 2 | Energy estimation of a sustainable system for CO_2 reduction to CO based on flow cell with acidic, near neutral and alkaline media and MEA based anion exchange membrane (unit: $kJ \cdot mol^{-1}$).

	Acidic	Near neutral	Alkaline	MEA
Equilibrium	260	260	260	260
Cathode energy loss	192	127	54	127
Anode energy loss	68	133	46	46
Ohmic loss	26	77	18	10
Side reaction	60	66	42	49
Gas separation	28	62	28	28
Electrolyte regeneration	0	0	1473	216
Total	634	725	1921	736

Supplementary Table 3 | Energy estimation of a sustainable system for CO_2 reduction to ethylene based on flow cell with acidic, near neutral and alkaline media and MEA based anion exchange membrane (unit: $kJ \cdot mol^{-1}$).

	Acidic	Near neutral	Alkaline	MEA
Equilibrium	1338	1338	1338	1338
Cathode energy loss	1442	1051	613	1051
Anode energy loss	405	799	278	278
Ohmic loss	154	463	110	58
Side reaction	1431	1565	1002	1168
Gas separation	90	349	90	90
Electrolyte regeneration	0	0	8837	1669
Total	4860	5565	12268	5652

Supplementary Table 4 | List of values used for the parameters in the model.

Symbol	Name	Value	Reference
$D_{\mathrm{H^+}}$	Diffusion coefficient of hydronium ion	$9.311 \times 10^{-9}\ \mathrm{m^2 \cdot s^{-1}}$	2
$D_{\mathrm{K^+}}$	Diffusion coefficient of K^+ ion	$1.957 \times 10^{-9}\ \mathrm{m^2 \cdot s^{-1}}$	26
$D_{\mathrm{OTf^-}}$	Diffusion coefficient of OTf^- ion	$0.863 \times 10^{-9}\ \mathrm{m^2 \cdot s^{-1}}$	30
$D_{\mathrm{OH^-}}$	Diffusion coefficient of OH^- ion	$5.273 \times 10^{-9}\ \mathrm{m^2 \cdot s^{-1}}$	26
ε_0	Permittivity of vacuum	$8.85 \times 10^{-12}\ \mathrm{F \cdot m^{-1}}$	
ε_r	Relative permittivity of water	80.1	26
ν	Kinematic viscosity of water	$1 \times 10^{-6}\ \mathrm{m^2 \cdot s^{-1}}$	3
k_{w1}	Rate constant of water dissociation	$2.4 \times 10^{-2}\ \mathrm{mol \cdot m^{-3} \cdot s^{-1}}$	26
k_{w2}	Rate constant of H^+-OH^- neutralization	$2.4 \times 10^{6}\ \mathrm{mol^{-1} \cdot m^3 \cdot s^{-1}}$	26
T	Temperature	$293\ \mathrm{K}$	
R	Ideal gas constant	$8.314\ \mathrm{J \cdot mol^{-1} \cdot K^{-1}}$	

Supplementary References

1 Levich, V. G. *Physicochemical Hydrodynamics*. (Prentice-Hall, Englewood Cliffs, 1962).

2 Atkins, P. W. & De Paula, J. *Physical Chemistry.* 7th edn, (Oxford University Press, 2002).

3 Grozovski, V., Vesztergom, S., Láng, G. G. & Broekmann, P. Electrochemical hydrogen evolution: H^+ or H_2O reduction? A rotating disk electrode study. *J. Electrochem. Soc.* **164**, E3171-E3178, (2017).

4 Huang, J. E. *et al.* CO_2 electrolysis to multicarbon products in strong acid. *Science* **372**, 1074-1078, (2021).

5 Paturska, A., Repele, M. & Bazbauers, G. Economic assessment of biomethane supply system based on natural gas infrastructure. *Energy Procedia* **72**, 71-78, (2015).

6 Jouny, M., Luc, W. & Jiao, F. General techno-economic analysis of CO_2 electrolysis systems. *Ind. Eng. Chem. Res.* **57**, 2165-2177, (2018).

7 Singh, M. R., Goodpaster, J. D., Weber, A. Z., Head-Gordon, M. & Bell, A. T. Mechanistic insights into electrochemical reduction of CO_2 over Ag using density functional theory and transport models. *Proc. Natl. Acad. Sci.* **114**, E8812-E8821, (2017).

8 Burdyny, T. *et al.* Nanomorphology-enhanced gas-evolution intensifies CO_2 reduction electrochemistry. *ACS Sustain. Chem. Eng.* **5**, 4031-4040, (2017).

9 Zhang, B. A., Ozel, T., Elias, J. S., Costentin, C. & Nocera, D. G. Interplay of homogeneous reactions, mass transport, and kinetics in determining selectivity of the reduction of CO_2 on gold electrodes. *ACS Centr. Sci.* **5**, 1097-1105, (2019).

10 Keith, D. W., Holmes, G., St. Angelo, D. & Heidel, K. A Process for capturing CO_2 from the atmosphere. *Joule* **2**, 1573-1594, (2018).

11 Ren, S. *et al.* Molecular electrocatalysts can mediate fast, selective CO_2 reduction in a flow cell. *Science* **365**, 367-369, (2019).

12 Oh, Y. & Hu, X. Organic molecules as mediators and catalysts for photocatalytic and electrocatalytic CO_2 reduction. *Chem. Soc. Rev.* **42**, 2253-2261, (2013).

13 Li, F. *et al.* Molecular tuning of CO_2-to-ethylene conversion. *Nature* **577**, 509-513, (2020).

14 Cao, L. *et al.* Dynamic oxygen adsorption on single-atomic ruthenium catalyst with high performance for acidic oxygen evolution reaction. *Nat. Commun.* **10**, 4849, (2019).

15 Zhang, L. *et al.* Boosting neutral water oxidation through surface oxygen modulation. *Adv. Mater.* **32**, 2002297, (2020).

16 Liang, C. *et al.* Exceptional performance of hierarchical Ni–Fe oxyhydroxide@NiFe alloy nanowire array electrocatalysts for large current density water splitting. *Energy Environ. Sci.* **13**, 86-95, (2020).

17 Jin, S., Hao, Z., Zhang, K., Yan, Z. & Chen, J. Advances and challenges for the electrochemical reduction of CO_2 to CO: From fundamentals to industrialization. *Angew. Chem. Int. Ed.* **60**, 20627-20648, (2021).

18 Gilliam, R. J., Graydon, J. W., Kirk, D. W. & Thorpe, S. J. A review of specific conductivities of potassium hydroxide solutions for various concentrations and temperatures. *Int. J. Hydrog. Energy* **32**, 359-364, (2007).
19 Kutz, R. B. *et al.* Sustainion imidazolium-functionalized polymers for carbon dioxide electrolysis. *Energy Technol.* **5**, 929-936, (2017).
20 Verma, S. *et al.* Insights into the low overpotential electroreduction of CO_2 to CO on a supported gold catalyst in an alkaline flow electrolyzer. *ACS Energy Lett.* **3**, 193-198, (2018).
21 Ruthven, D. M., Farooq, S. & Knaebel, K. S. *Pressure Swing Adsorption*. (Wiley, 1993).
22 Mahida, B., Benyounes, H. & Shen, W. Process analysis of pressure-swing distillation for the separation of formic acid–water mixture. *Chem. Papers* **75**, 599-609, (2021).
23 Selvaraj, H., Aravind, P. & Sundaram, M. Four compartment mono selective electrodialysis for separation of sodium formate from industry wastewater. *Chem. Eng. J.* **333**, 162-169, (2018).
24 Newman, J. & Thomas-Alyea, K. E. *Electrochemical Systems*. 3rd edn, (John Wiley & Sons, 2004).
25 Bard, A. J. & Faulkner, L. R. *Electrochemical Methods: Fundamentals and Applications*. 2nd edn, (John Wiley & Sons, 2001).
26 Bohra, D., Chaudhry, J. H., Burdyny, T., Pidko, E. A. & Smith, W. A. Modeling the electrical double layer to understand the reaction environment in a CO_2 electrocatalytic system. *Energy Environ. Sci.* **12**, 3380-3389, (2019).
27 Strmcnik, D. *et al.* Improving the hydrogen oxidation reaction rate by promotion of hydroxyl adsorption. *Nat. Chem.* **5**, 300-306, (2013).
28 Bode, D. D., Andersen, T. N. & Eyring, H. Anion and pH effects on the potentials of zero charge of gold and silver electrodes. *J. Phys. Chem.* **71**, 792-797, (1967).
29 Wuttig, A., Yaguchi, M., Motobayashi, K., Osawa, M. & Surendranath, Y. Inhibited proton transfer enhances Au-catalyzed CO_2-to-fuels selectivity. *Proc. Natl. Acad. Sci.* **113**, E4585-E4593, (2016).
30 Vanýsek, P. Ionic conductivity and diffusion at infinite dilution, in *Handbook of Chemistry and Physics*. (CRC Press, 1992).